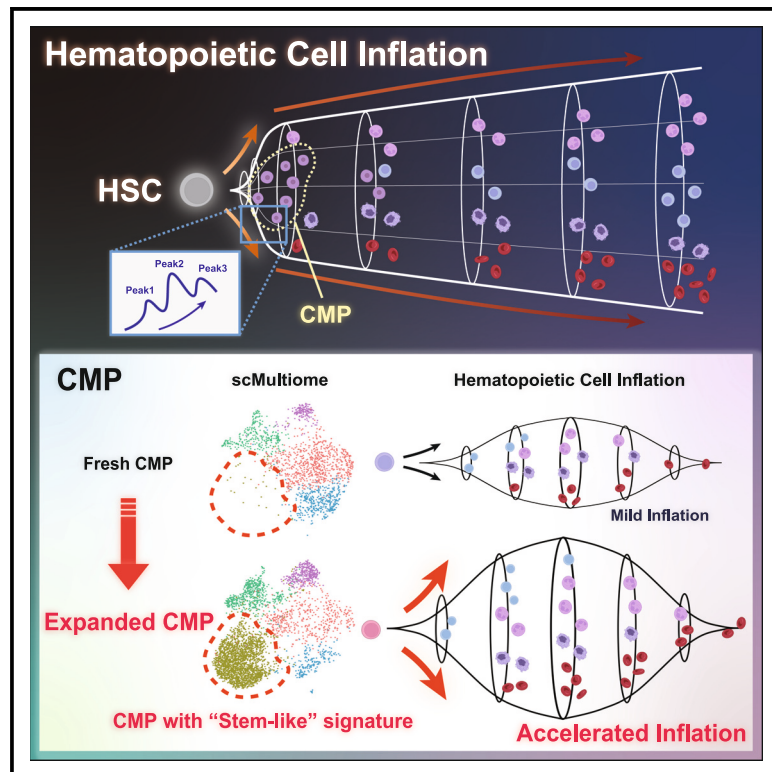


## Progenitor effect in the spleen drives early recovery via universal hematopoietic cell inflation

### Graphical abstract



### Authors

Takao Yogo, Hans Jiro Becker,  
Takaharu Kimura, ..., Toshio Suda,  
Atsushi Iwama, Satoshi Yamazaki

### Correspondence

takayogo0430@g.ecc.u-tokyo.ac.jp  
(T.Y.),  
y-sato4@g.ecc.u-tokyo.ac.jp (S.Y.)

### In brief

Using *in vivo* imaging, Yogo et al. revealed “hematopoietic cell inflation,” an early hematopoietic process driven by common myeloid progenitors (CMPs) after hematopoietic stem cell (HSC) transplantation. Expanded CMPs (exCMPs) with HSC-like signature accelerate this process in the spleen. Universal exCMPs enhance allogeneic hematopoiesis, offering therapeutic potential post transplantation.

### Highlights

- Hematopoietic cell inflation occurs in three peaks in the spleen after HSC transplantation
- CMPs act in concert with the spleen and accelerate hematopoietic cell inflation
- Expanded CMPs exhibit HSC-like signatures and accelerate hematopoietic cell inflation
- Universal expanded CMPs enhance early hematopoietic recovery in allogeneic transplantation



## Resource

# Progenitor effect in the spleen drives early recovery via universal hematopoietic cell inflation

Takao Yogo,<sup>1,2,\*</sup> Hans Jiro Becker,<sup>1,2</sup> Takaharu Kimura,<sup>1,2</sup> Satoshi Iwano,<sup>3</sup> Takahiro Kuchimaru,<sup>4</sup> Atsushi Miyawaki,<sup>5</sup> Tomomasa Yokomizo,<sup>6</sup> Toshio Suda,<sup>7,8</sup> Atsushi Iwama,<sup>9</sup> and Satoshi Yamazaki<sup>1,2,10,11,\*</sup>

<sup>1</sup>Division of Cell Regulation, Center for Experimental Medicine and Systems Biology, The Institute of Medical Science, The University of Tokyo, Tokyo, Japan

<sup>2</sup>Division of Cell Engineering, Center for Stem Cell Biology and Regenerative Medicine, The Institute of Medical Science, The University of Tokyo, Tokyo, Japan

<sup>3</sup>Institute for Tenure Track Promotion, University of Miyazaki, Miyazaki, Japan

<sup>4</sup>Center for Molecular Medicine, Jichi Medical University, Shimotsuke, Japan

<sup>5</sup>Laboratory for Cell Function Dynamics, RIKEN Center for Brain Science, RIKEN, Saitama, Japan

<sup>6</sup>Department of Microscopic and Developmental Anatomy, Tokyo Women's Medical University, Tokyo, Japan

<sup>7</sup>International Research Center for Medical Sciences, Kumamoto University, Kumamoto, Japan

<sup>8</sup>Stem Cell Biology Institute of Hematology, Blood Diseases Hospital Chinese Academy of Medical Sciences & Peking Union Medical College, Beijing, China

<sup>9</sup>Division of Stem Cell and Molecular Medicine, Center for Stem Cell Biology and Regenerative Medicine, The Institute of Medical Science, The University of Tokyo, Tokyo, Japan

<sup>10</sup>Laboratory for Stem Cell Therapy, Faculty of Medicine, Tsukuba University, Ibaraki, Japan

<sup>11</sup>Lead contact

\*Correspondence: takayogo0430@g.ecc.u-tokyo.ac.jp (T.Y.), y-sato4@g.ecc.u-tokyo.ac.jp (S.Y.)

<https://doi.org/10.1016/j.celrep.2025.115241>

## SUMMARY

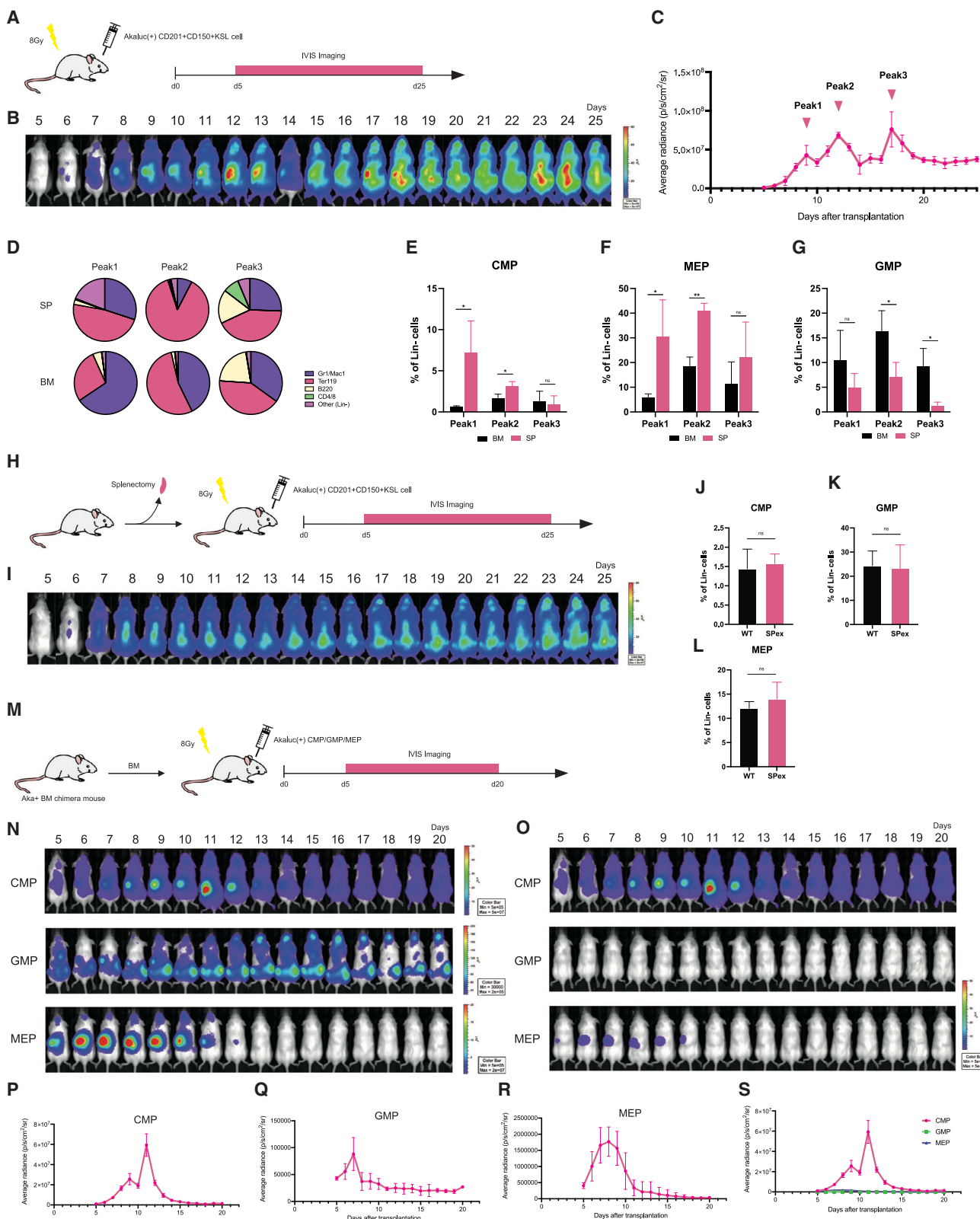
Hematopoietic stem cells (HSCs) possess the capacity to regenerate the entire hematopoietic system. However, the precise HSC dynamics in the early post-transplantation phase remain an enigma. Clinically, the initial hematopoiesis in the post-transplantation period is critical, necessitating strategies to accelerate hematopoietic recovery. Here, we uncovered the spatiotemporal dynamics of early active hematopoiesis, “hematopoietic cell inflation,” using a highly sensitive *in vivo* imaging system. Hematopoietic cell inflation occurs in three peaks in the spleen after transplantation, with common myeloid progenitors (CMPs), notably characterized by HSC-like signatures, playing a central role. Leveraging these findings, we developed expanded CMPs (exCMPs), which exhibit a gene expression pattern that selectively proliferates in the spleen and promotes hematopoietic expansion. Moreover, universal exCMPs supported early hematopoiesis in allogeneic transplantation. Human universal exCMPs have the potential to be a viable therapeutic enhancement for all HSC transplant patients.

## INTRODUCTION

Hematopoietic stem cells (HSCs) are tissue stem cells endowed with the capacity for self-renewal and multipotentiality, enabling them to regenerate the entire blood system after transplantation into a radiation- or chemotherapy-conditioned recipient.<sup>1,2</sup> Previously, we reported the impact of the bone marrow (BM) micro-environment in regulating the cell cycle dynamics of HSCs and have shown that the perturbation of *in vivo* amino acid balance enables HSC transplantation without prior treatment.<sup>3,4</sup> Although there have been many reports by our group and others on the analysis of HSCs in the BM under normal conditions, there are few reports on the process of BM reconstitution after HSC transplantation. In particular, the early spatiotemporal dynamics of transplanted HSCs within the body remain enigmatic.

In 1961, Till and McCulloch hypothesized the existence of HSCs based on the observation of colony formation following the transplantation of BM cells into irradiated mice.<sup>5</sup> Later investigations showed that different splenic colonies could be observed on days 7–8 and 10–12 after transplantation, and it has since been recognized that splenic colonies change on a daily basis.<sup>6</sup> Thus, even though the spleen undergoes significant changes in the early post-transplantation period, the biological function has remained a mystery for over half a century. One of the primary obstacles in analyzing hematopoietic kinetics during this period is the limitation of experimental systems. To date, the behavior of transplanted HSCs and their molecular mechanisms have been thoroughly investigated, but almost all studies have employed a “snapshot” analysis; i.e., mice are sacrificed at a specific time point and examined. Investigating the time course





(legend on next page)

of hematopoiesis within the same individual and at a whole-body scale has remained a challenge.

To address this issue, we focused on bioluminescence imaging systems, which have made remarkable progress in recent years. Utilizing the recently published, highly sensitive AkaLuc bioluminescence imaging system (AkaBLI), we visualized the *in vivo* dynamics of transplanted HSCs.<sup>7</sup> Our findings reveal that the spleen acts as a major site of vigorous and rapid hematopoiesis, “hematopoietic cell inflation,” and shows distinct hematopoietic patterns with dynamic changes. By tracking transplanted myeloid progenitors, we have discovered that common myeloid progenitors (CMPs) act in concert with the spleen and play a prominent role in hematopoietic cell inflation. Furthermore, we developed expanded CMPs (exCMPs) that leverage the splenic environment to improve early hematopoietic recovery after transplantation.

In clinical practice, many hematopoietic malignancies are curable only through BM transplantation; however, there are several obstacles that must be overcome to improve outcomes.<sup>8</sup> Significantly, fast reconstitution of hematopoietic cells is crucial, as it reduces the risk of infection and hemorrhage in the initial phase following HSC transplantation. HSCs must undergo multiple differentiation steps before mature blood cells emerge, impeding the rapid recovery of blood cell counts.<sup>9,10</sup> Although hematopoietic progenitors are expected to generate downstream mature cells more directly, their efficiency is limited, and innovative cell therapies for early hematopoietic recovery are in high demand. In this report, we identified a fraction of hematopoietic stem and progenitor cells (HSPCs) with distinct molecular patterns that play a crucial role in early hematopoietic recovery and developed universal HSPCs capable of massive production of myeloid cells shortly after transplantation.

A significant obstacle to widespread use of cell therapy is the delivery of a uniform batch to multiple patients. To address this, recent investigations have focused on the concept of universalization for cell therapy. One proposed approach to universalization involves deletion of the human leukocyte antigen (HLA) gene, as reported by several research groups.<sup>11,12</sup> However, the lack of HLA triggers a response from natural killer (NK) cells.<sup>13</sup> To avoid this unwanted response, HLA pseudo-homozygous cells, HLA-C retained cells, or HLA-E overexpressed cells

have been developed. Nonetheless, the complete suppression of T cell and NK cell activities continues to present a challenge, and, while universal cell therapy holds immense promise as a next-generation therapy, numerous issues must be resolved.<sup>14</sup> However, in the case of HSC transplantation, the recipients are in a state of immunological suppression with high-dose chemotherapy and whole-body irradiation, providing an ideal environment for recent universal cell therapies. In fact, universal exCMPs with knocked-out major histocompatibility complex (MHC) via CRISPR-Cas9 have demonstrated the ability to generate high numbers of blood cells and support hematopoietic recovery following allogeneic transplantation. The universal exCMPs developed in this study can be transplanted to any patient after appropriate conditioning, indicating potential for future clinical applications of “off-the-shelf” universal exCMPs as a cell product with immediate efficacy for rapid blood cell recovery.

## RESULTS

### CMPs act in concert with the spleen and initiate hematopoietic cell inflation

We applied the AkaBLI system to HSCs and integrated luminescence 2D/3D images with computed tomography (CT) scans to capture the spatial dynamics of early hematopoiesis on a whole-body scale after transplantation. Expanded C57BL/6 murine HSCs transduced with the *Akaluc* gene were transplanted into irradiated congenic recipients, which resulted in intense hematopoiesis in the spleen early after the transplantation (Figures S1A and S1B). Next, we transplanted Akaluc<sup>+</sup> CD150<sup>+</sup>CD201<sup>+</sup>cKit<sup>+</sup>Sca1<sup>+</sup>Lineage<sup>-</sup> (KSL) cells, which possess long-term BM reconstitution ability, and analyzed bioluminescence signals to elucidate the dynamics of cellular distributions over time (Figures 1A, S1C, and S1D). Our data reveal that the spleen is the main site of hematopoiesis and exhibits distinct hematopoietic patterns with dynamic changes, culminating in hematopoietic cell inflation that consisted of three peaks on days 9–10, 12, and 17–19 post transplantation (Figures 1B, 1C, and S1E). Further analysis of the spleen and BM cells using flow cytometry revealed that hematopoietic cells present in the spleen underwent significant changes over time. During the first peak, myeloid progenitors and neutrophils/macrophages proliferated,

---

### Figure 1. CMPs act in concert with the spleen and induce hematopoietic cell inflation

- (A) Schematic illustrating the analysis of hematopoietic dynamics after HSC transplantation with AkaBLI. Luminescence signals were measured by In Vivo Imaging System (IVIS) from day 5 to day 25 after transplantation of Akaluc<sup>+</sup>CD201<sup>+</sup>CD150<sup>+</sup>KSL cells into mice.
- (B) Representative IVIS image data obtained from day 5 to day 25.
- (C) Changes in mean luminescence intensity in the spleen after transplantation ( $n = 3$ ). Error bars represent SD.
- (D) Proportion of blood cells present in the spleen and BM at each hematopoietic peak ( $n = 3$ ). Error bars represent SD. \* $p < 0.05$  and \*\* $p < 0.01$  by two-tailed independent t test.
- (E–G) Percentage of myeloid progenitor cells, including CMPs (E), MEPs (F), and GMPs (G), present in the spleen and BM at each hematopoietic peak ( $n = 3$ ). Error bars represent SD. \* $p < 0.05$  and \*\* $p < 0.01$  by two-tailed independent t test.
- (H) Schematic illustrating the analysis of hematopoietic dynamics after HSC transplantation in splenectomized mice with AkaBLI.
- (I) Representative IVIS image data obtained from splenectomized mice from day 5 to day 25.
- (J–L) Percentage of myeloid progenitor cells, including CMPs (J), GMPs (K), and MEPs (L), present in the BM ( $n = 4$ ). SPex refers to splenectomized mice. Error bars represent SD. \* $p < 0.05$  and \*\* $p < 0.01$  by two-tailed independent t test.
- (M) Schematic illustrating the analysis of hematopoietic dynamics after myeloid progenitor transplantation with AkaBLI.
- (N and O) Representative IVIS image data obtained from each myeloid progenitor-transplanted mouse from day 5 to day 20 (N) and comparison of luminescent signal intensity (O).
- (P–S) Time course of average luminescence intensity in the spleen after transplantation of each myeloid progenitor cell, including CMPs (P), GMPs (Q), MEPs (R), and all (S) ( $n = 3$ ). Error bars represent SD.

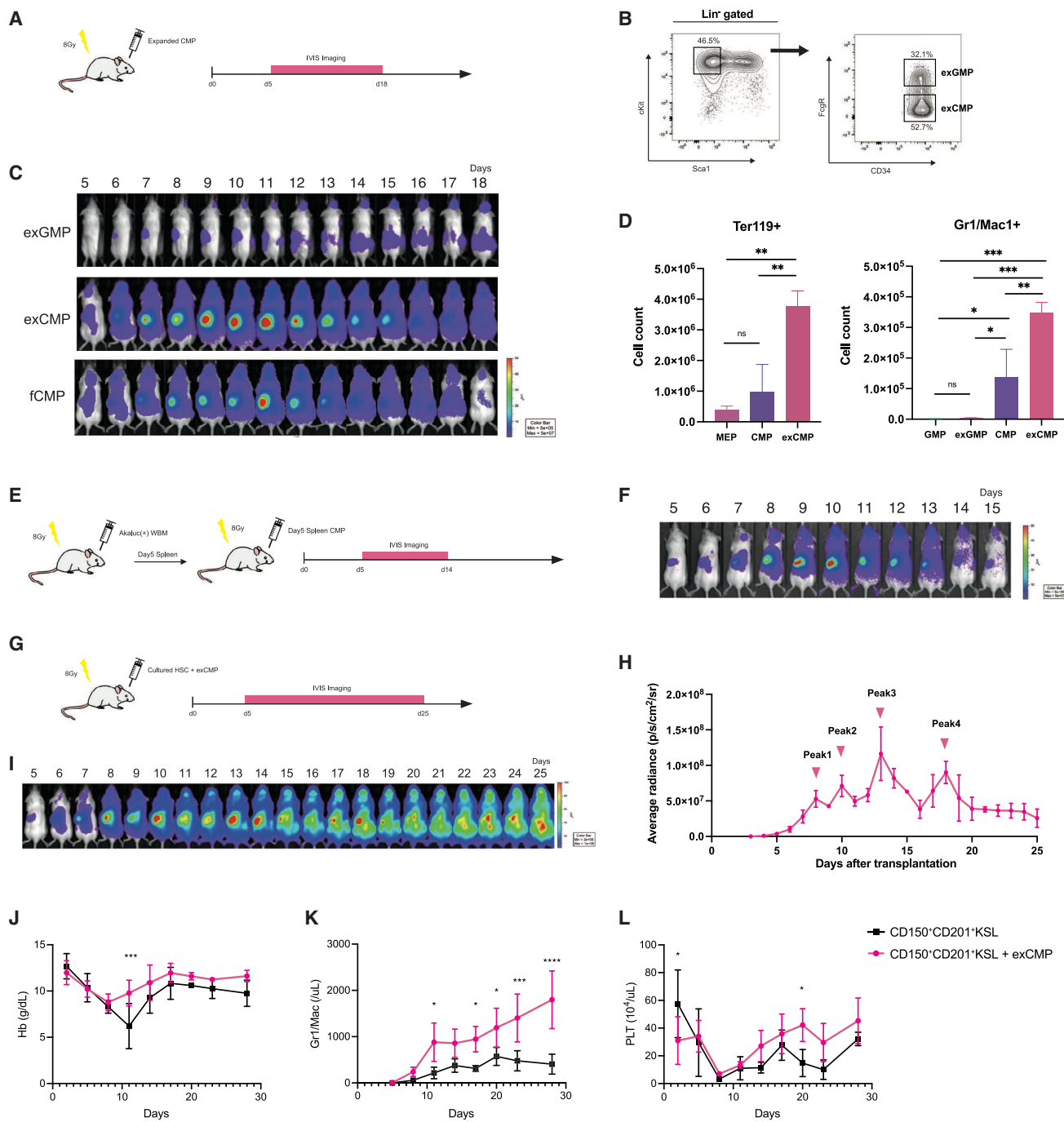


**Figure 2. Expanded CMPs accelerate hematopoietic cell inflation and support early hematopoietic recovery**

(A) Schematic illustrating the analysis of hematopoietic dynamics after exCMP transplantation with AkalucBLI. Luminescence signals were measured by IVIS from day 5 to day 18 after transplantation of exCMPs into mice.

(B) Representative FACS plot of exCMPs/exGMPs within Lin<sup>-</sup> cells.

(C) Representative IVIS imaging results obtained after transplantation of exCMPs/exGMPs/fCMPs.

(D) Comparison of the number of erythrocytes (Ter119<sup>+</sup>) and myelocytes (Gr1/Mac1<sup>+</sup>) produced by GMPs, MEPs, CMPs, exCMPs, and exCMPs in the spleen on day 7 after transplantation ( $n = 3$ ). Error bars represent SD. \* $p < 0.05$ , \*\* $p < 0.01$ , \*\*\* $p < 0.001$ , and \*\*\*\* $p < 0.0001$  by one-way ANOVA with Tukey's multiple comparison test.

(E) Schematic illustrating the SPaCMP transplantation experiment; Akaluc<sup>+</sup> SPaCMPs were harvested from the spleen on day 5 from Akaluc BM chimera mice. Luminescence signals were measured by IVIS from day 5 to day 15 after transplantation.

(F) Representative IVIS imaging results obtained after transplantation of SPaCMPs.

(legend continued on next page)

while erythrocytes dominated the second peak. During the third peak, cells of all lineages, including T cells, B cells, neutrophils/macrophages, and erythrocytes, appeared (Figures 1D and S1G–S1K). The spleen and BM underwent distinct hematopoietic transformations, with mature neutrophil/macrophages predominating in the BM, whereas myeloid progenitors and erythroid cells dominated in the spleen (Figures 1D and S1G–S1K). Notably, CMPs and megakaryocyte-erythroid progenitors (MEPs) were 11.0- and 5.2-fold more abundant in the spleen than in the BM during the first peak (Figures 1E–1G and S1F). A comprehensive analysis of each HSPC fraction indicated that the CMP, pre-granulocyte-macrophage (pre-GM), and pre-megakaryocyte/erythroid (pre-Mk/E) fractions increased significantly in the spleen compared to the BM at 7 days post transplantation (Figure S1L). The increase in CMP in the spleen was transient, and the percentage of CMPs at 28 days post transplantation was higher in the BM than in the spleen (Figure S1L). Next, we investigated the presence of hematopoietic cell inflation in organs other than the spleen using splenectomized mice (Figure 1H). As a result, there was no rapid hematopoiesis in splenectomized mice anywhere in the body (Figure 1I). We compared the percentage of myeloid progenitor cells (CMP, granulocyte-macrophage progenitor [GMP], and MEP) in the BM on day 9 post transplantation between normal and splenectomized mice, and no significant difference was observed in any progenitor cell type (Figures 1J–1L), indicating that the BM was unable to compensate for hematopoiesis in the spleen. Peripheral blood analysis showed that the recovery of hemoglobin (Hb) levels and Gr1/Mac1<sup>+</sup> cells was notably delayed in splenectomized mice (Figures S1M–S1O). These data demonstrate that hematopoietic cell inflation is a spleen-specific phenomenon that plays a crucial role in the initial explosive recovery of blood cells.

Next, we hypothesized that the three peaks of hematopoietic cell inflation in the spleen originate from myeloid progenitor cells that are located downstream of HSCs. We conducted transplants of each myeloid progenitor cell population (CMP/GMP/MEP) from Akaluc BM chimera mice and analyzed the luminescence signals over time (Figures 1M and S1P). As a result, GMPs are predominantly hematopoietic in the BM, while CMPs and MEPs utilize the spleen as a site for hematopoietic cell inflation (Figures 1N, 1P–1R, and S1Q). Rapid hematopoiesis by any of these progenitors vanished by 20 days after transplantation. Importantly, CMPs generated significantly more blood cells than MEPs or GMPs (Figures 1O and 1S). Thus, our detailed analysis shows that CMPs play a pivotal role in hematopoietic recovery, which is consistent with the phenomenon of spleen-specific CMPs observed early after HSC transplantation. Consequently, we surmise that CMPs are key to generating early post-transplant hematopoietic cell inflation.

### exCMPs accelerate hematopoietic cell inflation

We examined the post-transplantation kinetics of cultured myeloid progenitors. Following the expansion of murine HSCs *in vitro*,<sup>15</sup> we obtained expanded GMPs (exGMPs) and exCMPs from the CD34<sup>+</sup>FcgR<sup>+</sup>KSL and CD34<sup>+</sup>FcgR<sup>-</sup>KSL fractions, respectively. The luminescence signals were analyzed after transplantation of Akaluc<sup>+</sup> exGMP or Akaluc<sup>+</sup> exCMPs (Figures 2A and 2B), revealing that exCMPs induced hematopoietic cell inflation in the spleen and produced more cells than exGMPs (Figure 2C). Seven days after transplantation, exGMPs differentiated into neutrophils and macrophages, while exCMPs differentiated into neutrophils, macrophages, and erythrocytes, thus demonstrating a differentiation capacity similar to steady-state GMPs (fresh GMP) and CMPs (fresh CMPs [fCMPs]) (Figure S2A). Notably, we found that exCMPs could induce hematopoietic cell inflation much earlier than fCMPs (Figures 2C and S2B) and produced significantly more cells after the injection of equal cell numbers (Figure 2D). The hematopoiesis by exCMPs was transient, with 0% chimerism after 4 weeks (Figure S2C).

We next focused on CMPs that appear in the spleen early after transplantation (spleen-activated CMPs [SPaCMPs]). Following BM transplantation, the percentage of CMPs reaches its maximum on day 5 (Figures S2D and S2E). We collected SPaCMPs from the spleen on day 5 after BM transplantation, transplanted them into another irradiated recipient, and examined the dynamics of SPaCMPs using In Vivo Imaging System (IVIS) imaging (Figure 2E). Our findings indicate that SPaCMPs, similar to exCMPs, induced hematopoietic cell inflation in the spleen earlier than fCMPs (Figure 2F) and produced a large number of cells in the short term (Figures S2F and S2G). Therefore, exCMPs in culture and SPaCMPs in mice display distinct kinetics from fCMPs after transplantation, leading to the acceleration of hematopoietic cell inflation in the spleen while retaining the same differentiation potential as CMPs.

We expected that the addition of exCMPs would facilitate faster post-transplant hematopoietic recovery than HSCs alone. Therefore, we transplanted a combination of 10,000 exCMPs and 3,000 cultured HSCs (CD150<sup>+</sup>CD201<sup>+</sup>KSL cells) into irradiated mice and analyzed post-transplant hematopoiesis dynamics using the AkaBLI system (Figure 2G). As expected, hematopoietic cell inflation occurred earlier with the addition of exCMPs than with HSCs alone (Figures 2H, 2I, and S2D). Peripheral blood analysis showed an earlier recovery of Hb levels, as well as neutrophil, macrophage, and platelet counts, following transplantation of the exCMP mixture (Figures S2K and S2L). In the case of splenectomized mice, the recovery of blood cells was notably delayed (Figures S2H–S2J), indicating that exCMPs work in concert with the spleen to aid in early hematopoietic recovery.

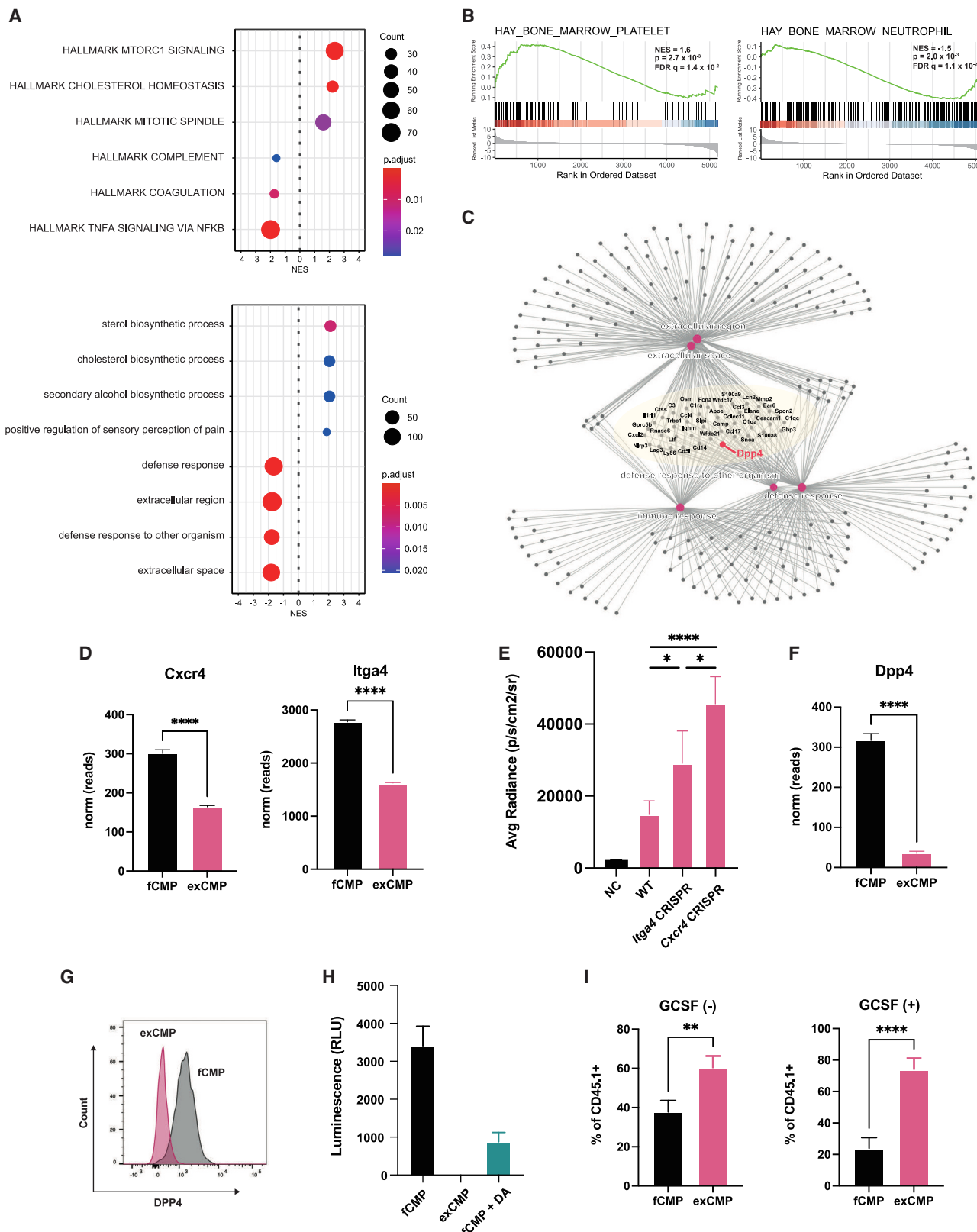
To assess whether human CMPs could be expanded similarly, we cultured human cord blood CD34<sup>+</sup> cells in previously

(G) Schematic illustrating mixed transplantation with exCMPs. Akaluc<sup>+</sup> exCMPs and HSCs were transplanted into irradiated mice, and luminescence signals were measured from day 5 to day 25.

(H) Changes in average luminescence intensity in the spleen after transplantation ( $n = 3$ ). Error bars represent SD.

(I) Representative IVIS imaging results obtained after transplantation of exCMPs and HSCs.

(J–L) Blood cell counts, including Hb (J), Gr1/Mac1<sup>+</sup> cells (K), and platelets (L), in peripheral blood with and without exCMPs on day 10 after transplantation ( $n = 5$ ). Error bars represent SD. \* $p < 0.05$ , \*\* $p < 0.01$ , \*\*\* $p < 0.001$ , and \*\*\*\* $p < 0.0001$  by two-way ANOVA with Tukey's multiple comparison test.



(legend on next page)

reported conditions.<sup>16,17</sup> StemRegenin 1 (SR1) amplification of CMPs was more efficient than nicotinamide, resulting in a significant increase in cell numbers by more than 11-fold within 2 weeks (Figures S2K and S2L). Human exCMPs underwent short-term hematopoiesis in NOD/Shi-scid,IL-2R $\gamma$ KO (NOG) mice (Figure S2M) and produced myeloid cells, similar to murine exCMPs (Figures S2N and S2O). These findings indicate that, as in the murine model, human exCMP can also be easily expanded ex vivo and facilitate short-term rapid hematopoiesis.

#### exCMPs select the spleen and proliferate efficiently in response to cytokines

To initiate early hematopoietic cell inflation, exCMPs need to choose the spleen, rather than the BM as the site for rapid proliferation. To unravel the underlying mechanism responsible for the remarkable capability of exCMPs, we compared gene expression patterns using bulk RNA sequencing (RNA-seq) (Figures 3A–3C and S3A). First, we discovered that the expression of *Cxcr4* and *Itga4*, which are pivotal in BM homing, was notably reduced in exCMPs compared to fCMPs (Figure 3D). Homing efficacy of exCMPs to the spleen further intensified when *Cxcr4* or *Itga4* was knocked out (Figures 3E, S3B, and S3C), indicating that exCMPs select the spleen due to lower *Cxcr4* and *Itga4* expression levels. Second, the expression of *Dpp4*, a serine protease, was also substantially reduced in exCMPs, with no DPP4 enzymatic activity (Figures 3C–3H). DPP4 is known to hamper the effects of granulocyte colony stimulating factor (G-CSF) and erythropoietin (EPO) by cleaving them.<sup>18</sup> Thus, we compared the response of exCMPs and fCMPs to G-CSF in mice by transplanting both into the same irradiated mice and administering G-CSF after transplantation (Figure S3D). As anticipated, the chimerism of exCMPs significantly increased when G-CSF was administered, indicating that exCMPs are more sensitive to G-CSF than fCMPs *in vivo* (Figures 3L and S3E). Furthermore, exCMPs exhibited enrichment of platelet-related gene expression compared to fCMPs, whereas fCMPs showed enrichment of neutrophil-related genes, and activation of MTORC1 signaling was detected in exCMPs, indicative of their activated state (Figures 3A and 3B). In conclusion, our findings suggest that exCMPs can efficiently initiate early hematopoietic cell inflation by selectively homing to the spleen rather than the BM and by efficiently responding to cytokines.

#### CMPs exhibiting stem cell signature drive intense hematopoietic cell inflation

The heterogeneity of CMPs has been well documented in previous studies employing single-cell RNA-seq technology.<sup>19</sup> To analyze the heterogeneity of exCMPs and SPaCMPs, we conducted single-cell multiome analysis on individual CMPs, comparing exCMPs with fCMPs from the BM and SPaCMPs derived from the spleens of mice following HSC transplantation (Figure 4A). Strikingly, this analysis revealed a previously uncharacterized population of cells that, while being progenitor cells, exhibit stem cell signatures (Figures 4B–4D and S4A–S4C). Within this cluster, HSC-specific genes such as *Hlf*, *Mecom*, and *Fgd5* were upregulated, while genes like *Mpo* and *Gata1* were downregulated (Figures 4D and S4A–S4C). Notably, this population was observed at a particularly high frequency in exCMPs (Figures 4C and S4B). Chromatin accessibility analysis across clusters unveiled differential accessibility for genes such as *Gata1* and *Ly6c2*; however, *Hlf* remained accessible in clusters beyond *Hlf*+ CMPs, suggesting the possibility of transcription factor-mediated regulation of gene expression (Figures 4E and S4D). We hypothesized that *Hlf*+ CMPs play a pivotal role in hematopoietic cell inflation and investigated their function using *Hlf*-tdTomato reporter mice. Fluorescence-activated cell sorting (FACS) analysis revealed that 16.2% of exCMPs were *Hlf*-tdTomato positive (Figure 4F). Luminescence signals were analyzed post transplantation of Akaluc<sup>+</sup> *Hlf*-High exCMPs or Akaluc<sup>+</sup> *Hlf*-Low exCMPs, demonstrating that *Hlf*-High exCMPs induced more intense hematopoietic cell inflation in the spleen and generated a greater number of cells compared to *Hlf*-Low exCMPs (Figures 4H, 4G, S4E, and S4F). Additionally, we confirmed that exCMPs retained the same differentiation potential as CMPs, differentiating into GMPs and MEPs, as well as Gr1/Mac1<sup>+</sup> cells and Ter119<sup>+</sup> cells (Figures S4G and S4H). In conclusion, our findings suggest that the *Hlf*-High CMP population, which is enriched during *ex vivo* expansion, is capable of driving more intense hematopoietic cell inflation post transplantation, reflecting the distinct functional properties of exCMPs.

#### Spleen-dependent “progenitor effect” allows long-term survival in the absence of HSC

exCMPs exhibit the ability to undergo hematopoietic cell inflation and hematopoietic shrinkage in the spleen after transplantation, leading to transient but rapid and vigorous hematopoiesis.

**Figure 3. exCMPs selectively target the spleen and efficiently proliferate in response to cytokines**

- (A) Gene Ontology analysis of exCMPs and fCMPs using bulk RNA-seq.
- (B) Gene set enrichment analysis (GSEA) of exCMPs and fCMPs.
- (C) Gene Ontology network analysis of exCMPs and fCMPs.
- (D) Comparison of *Cxcr4*/*Itga4* gene expression levels between exCMPs and fCMPs ( $n = 3$ ). Error bars represent SD. \* $p < 0.05$ , \*\* $p < 0.01$ , \*\*\* $p < 0.001$ , and \*\*\*\* $p < 0.0001$  by two-tailed independent t test.
- (E) Comparison of luminescence intensity in the spleen 24 h after Akaluc<sup>+</sup> WT ( $n = 4$ )/*Cxcr4* CRISPR ( $n = 4$ )/*Itga4* CRISPR ( $n = 3$ ) exCMP transplantation. Error bars represent SD. \* $p < 0.05$ , \*\* $p < 0.01$ , \*\*\* $p < 0.001$ , and \*\*\*\* $p < 0.0001$  by one-way ANOVA with Tukey's post-test.
- (F) Comparison of *Dpp4* gene expression levels between exCMPs and fCMPs ( $n = 3$ ). Error bars represent SD. \* $p < 0.05$ , \*\* $p < 0.01$ , \*\*\* $p < 0.001$ , and \*\*\*\* $p < 0.0001$  by two-tailed independent t test.
- (G) Comparison of DPP4 protein expression levels by flow cytometry between exCMPs and fCMPs.
- (H) Comparison of DPP4 activity levels between exCMPs and fCMPs (exCMP  $n = 7$ , fCMP  $n = 4$ , fCMP+DA  $n = 4$ ). DPP4 enzyme activity was determined by means of the DPP4-Glo Protease Assay (Promega).
- (I) Percentage of cells derived from fCMPs and exCMPs in the spleen on day 7 post transplantation with and without G-CSF administration. Error bars represent SD. \* $p < 0.05$ , \*\* $p < 0.01$ , \*\*\* $p < 0.001$ , and \*\*\*\* $p < 0.0001$  by two-tailed independent t test.

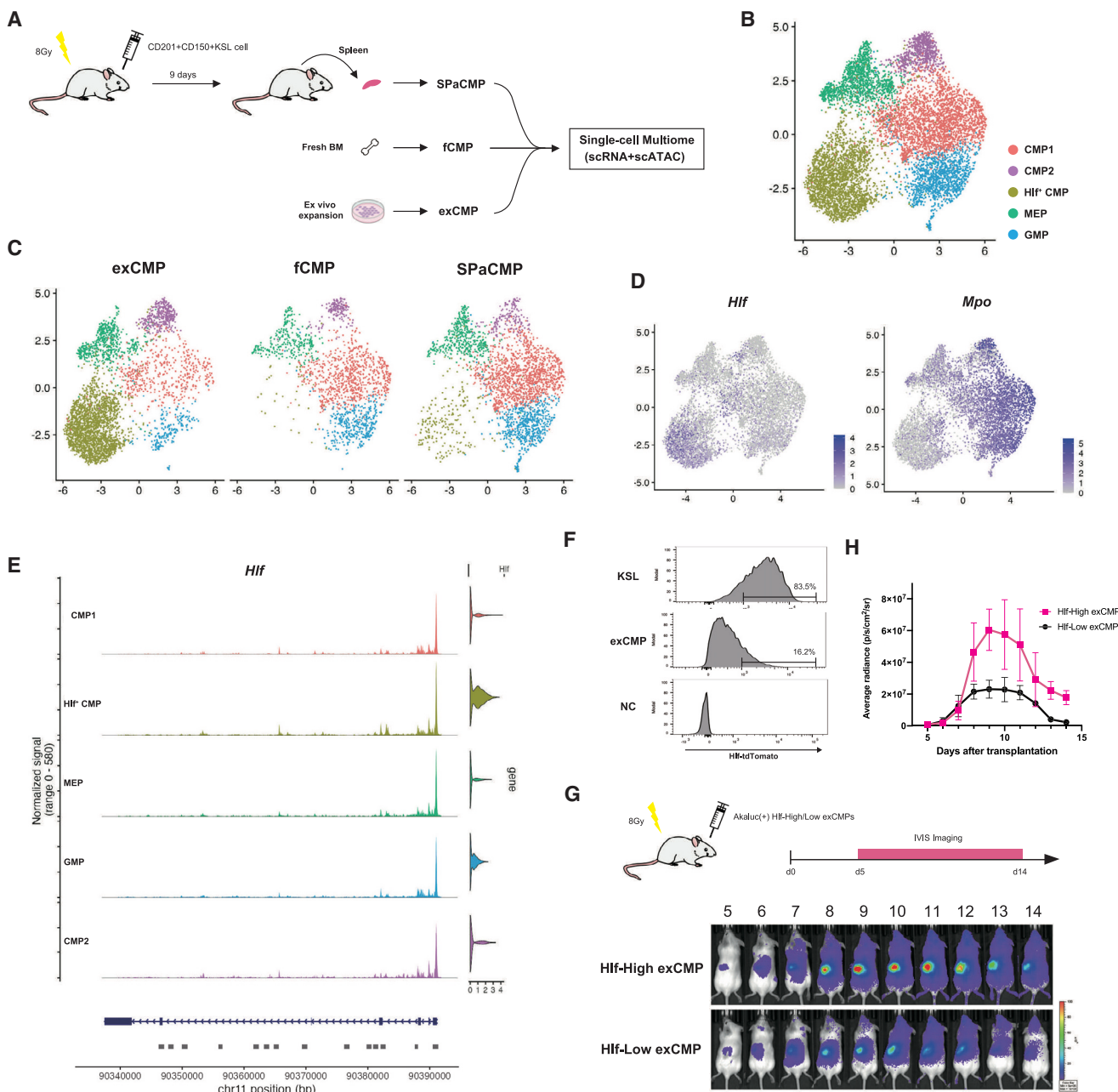


**Figure 4. Single-cell multiome analysis reveals enrichment of Hif+ CMPs within exCMP population**

- (A) Protocol for single-cell multiome analysis of SPaCMPs, fCMPs, and exCMPs. SPaCMPs were collected from the spleen 9 days following HSC transplantation, fCMPs were directly collected from BM, and exCMPs were collected from HSCs cultured for 7 days.
- (B) Uniform manifold approximation and projection (UMAP) plot of scRNA-seq data with five cell clusters annotated. Integrated cell map from exCMPs, fCMPs, and SPaCMPs.
- (C) Distribution of cells within exCMPs, fCMPs, and SPaCMPs.
- (D) Feature plots showing the expression of *Hif* and *Mpo* genes within the integrated cell map.
- (E) Chromatin-accessible regions and corresponding gene expression of *Hif*.
- (F) Hif-tdTOMO high population within KSL (top), exCMPs (middle), and negative control (bottom).
- (G) Schematic illustrating the analysis of hematopoietic dynamics following transplantation of Hif-High/Low exCMPs with AkaBLI. Luminescence signals were measured using IVIS from day 5 to day 14 post transplantation.
- (H) Dynamic changes in mean luminescence intensity in the spleen after transplantation of Hif-High/Low exCMPs ( $n = 4$ ). Error bars represent SD.

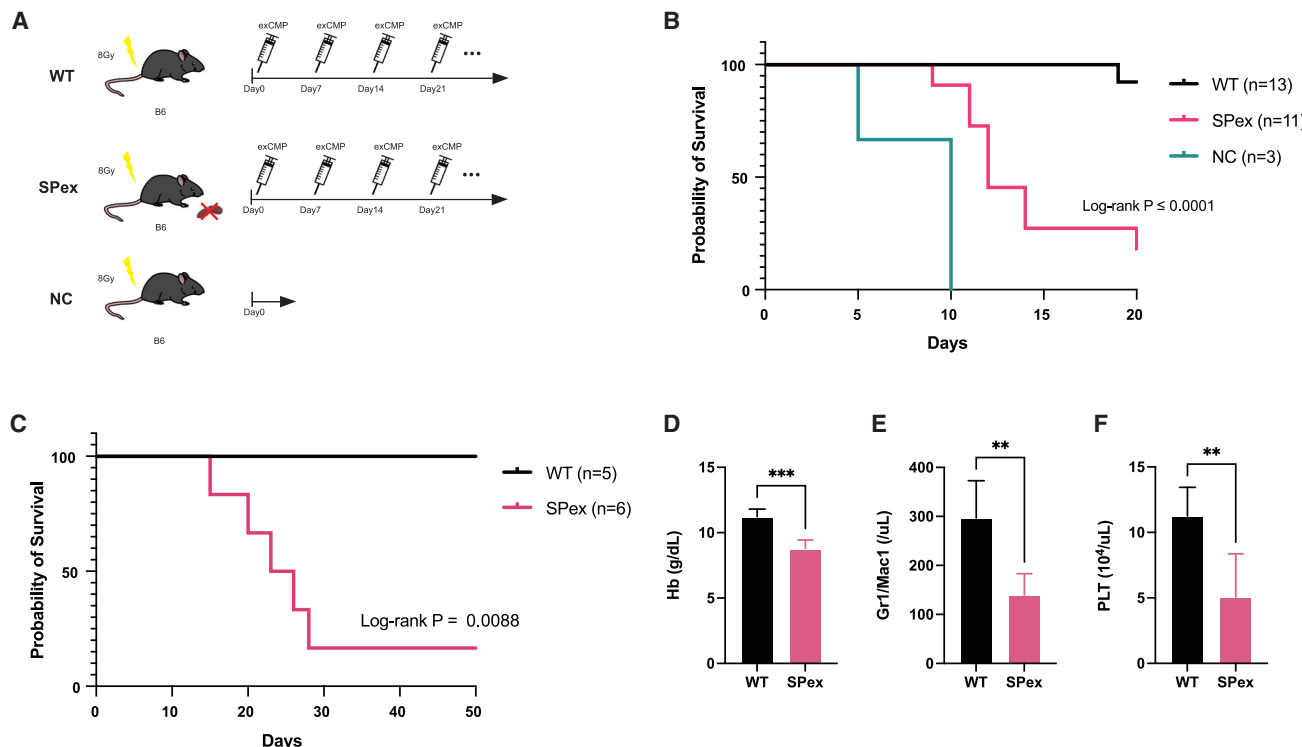


**Figure 5. Weekly transplantation of exCMPs supports long-term hematopoiesis without HSCs**

(A) Schematic of repetitive exCMP transplantation. exCMPs were transplanted to lethally irradiated mice once a week.  
(B) Survival curve of irradiated mice transplanted with 30,000 exCMPs weekly. The log-rank test was used to determine survival difference between groups.  
(C) Survival curve of irradiated mice transplanted with 100,000 exCMPs weekly. The log-rank test was used to determine survival difference between groups.  
(D–F) Hemoglobin levels (D), the number of Gr1/Mac1<sup>+</sup> cells (E), and platelet counts (F) in the peripheral blood on day 10 after weekly transplantation of 100,000 exCMPs (WT n = 5, SPex n = 6). Error bars represent SD. \*p < 0.05, \*\*p < 0.01, and \*\*\*p < 0.001 by two-tailed independent t test.

Building upon this intrinsic progenitor effect, we hypothesized that repeated administration of exCMPs could supply a sufficient number of hematopoietic cells for survival, even in the absence of HSCs. Thus, we administered 30,000 or 100,000 exCMPs alone to lethally irradiated mice on a weekly basis (Figure 5A). Remarkably, this approach led to successful long-term survival of mice (Figures 5B and 5C). However, in splenectomized mice, long-term rescue was unsuccessful (Figures 5B and 5C). Furthermore, Hb levels, neutrophil and macrophage counts, and platelet counts were all significantly lower in the splenectomized mice (Figures 5D–5F). Collectively, these findings indicate that exCMPs are capable of life-sustaining blood cell production via a spleen-dependent progenitor effect and showcase their potential to enhance hematopoietic recovery by leveraging hematopoietic cell inflation.

#### Universal exCMPs accomplish hematopoietic cell inflation following allogeneic transplantation

Subsequently, we investigated the feasibility of allogeneic transplantation of exCMPs. We transplanted 100,000 Akaluc<sup>+</sup> exCMPs obtained from C57BL/6Ncr mice into irradiated BALB/c mice and recorded luminescence signals on day 5. Our results indicated that early hematopoiesis occurred in the spleens of C57BL/6Ncr mice, while no signal was detected in the spleens of BALB/c mice; hematopoietic signals were only

observed in BM (Figures S5A and S5B). We surmised that this disparity was caused by immune rejection in an allogeneic setting, wherein the spleen acts as an immune tissue rather than a hematopoietic tissue. Therefore, we proposed that the universalization of exCMPs could be a viable option for allogeneic transplantation. To achieve this, we created universal exCMPs (UNexCMPs) by knocking out the B2m gene using the CRISPR-Cas9 system (Figure 6A). The spleen of mice transplanted with UNexCMPs demonstrated hematopoiesis as early as 5 days after transplantation, and the signal was enhanced on day 7 (Figures 6B and 6C). Furthermore, UNexCMPs generated more cells than non-universalized exCMPs (Figure 6D). Additionally, UNexCMPs differentiated into MHC class I (−) erythroblasts, neutrophils, and macrophages after transplantation (Figures S5C and S5D). These findings indicate that UNexCMPs can use the spleen as a site of hematopoiesis and initiate hematopoietic cell inflation after allogeneic transplantation. We hypothesized that repetitive allogeneic transplantation of UNexCMPs could provide enough blood cells for survival in the absence of HSCs. Therefore, we transplanted UNexCMPs from C57BL/6Ncr mice or non-universalized wild-type (WT) exCMPs (100,000 cells) into BALB/c mice weekly (Figure 6E). As expected, mice transplanted with WTexCMPs did not survive beyond 2 weeks, whereas all mice transplanted with UNexCMPs survived long term (Figure 6F). Thus, the universalization of

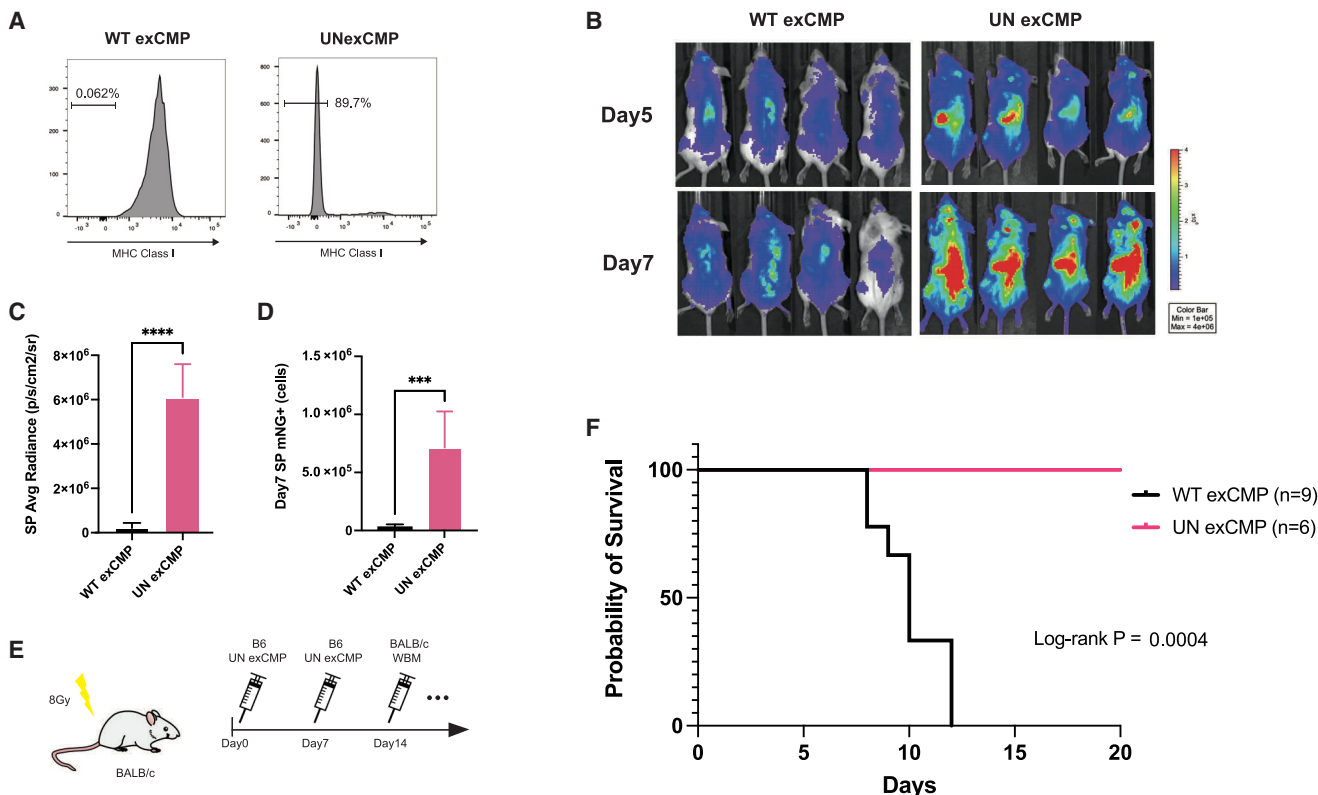


**Figure 6. Universal exCMPs promote hematopoietic cell inflation after allogeneic transplantation**

- (A) MHC class I expression of WT exCMPs and UNexCMPs.  
 (B) IVIS image results of Akaluc<sup>+</sup> WT exCMPs/UNexCMPs from C57BL/6 mice transplanted into irradiated BALB/c mice on days 5 and 7.  
 (C) Luminescence intensity in the spleen on day 7 after transplantation ( $n = 4$ ). Error bars represent SD. \* $p < 0.05$ , \*\* $p < 0.01$ , \*\*\* $p < 0.001$ , and \*\*\*\* $p < 0.0001$  by two-tailed independent t test.  
 (D) Number of mNeon-Green (mNG)-positive cells in the spleen on day 7 after transplantation (WT exCMP  $n = 4$ , UNexCMP  $n = 7$ ). Error bars represent SD. \* $p < 0.05$ , \*\* $p < 0.01$ , \*\*\* $p < 0.001$ , and \*\*\*\* $p < 0.0001$  by two-tailed independent t test.  
 (E) Schematic of UNexCMP repetitive transplantation.  
 (F) Survival curves of WT exCMPs/UNexCMPs repetitively transplanted into irradiated BALB/c mice. The log-rank test was used to determine survival difference between groups.

exCMPs, which enables early hematopoietic cell inflation, facilitates flexible control of hematopoietic recovery in allogeneic transplantation. To confirm whether human exCMPs could be universalized, we knocked out the *B2M* gene in human exCMPs expanded in SR1-supplemented cultures. Similar to mice, we were able to create human universal exCMPs with an efficiency of over 80% (Figure S5E). The transplanted universal exCMPs underwent short-term hematopoiesis in NOG mice, producing myeloid cells (Figure S5F). Consequently, we anticipate that human universal exCMPs function similarly to mouse exCMPs in the human system.

## DISCUSSION

Numerous previous investigations have employed various techniques, including immunostaining, flow cytometry, and RNA-seq, to examine the hematopoietic activity of transplanted cells. However, these methods require sacrificing mice and collecting tissues from specific organs at set time points, making it impractical for long-term analysis in the same individual. Kim et al.

addressed this limitation by employing the tibia window technique, which permits direct observation of the BM through fluorescent imaging; however, this invasive approach limits the analysis to a small part of the BM.<sup>20</sup> Although luminescence imaging using D-Luciferin/Fluc is a noninvasive method to observe luminescence signals over time in the same organism, the intensity of the luminescence is weak and inaccurate.<sup>21,22</sup> Therefore, a more sensitive technique was necessary to analyze post-transplant hematopoiesis. In this study, we utilized AkaBLI to investigate the spatiotemporal dynamics of post-transplant hematopoiesis and determined that the spleen is the primary organ responsible for hematopoietic cell inflation. Hematopoietic cell inflation consists of three hematopoietic peaks, and we discovered that hematopoiesis in the spleen changes over time. This study examines splenic hematopoiesis and its changes, historically documented as splenic colonies since the 1960s, using a state-of-the-art luminescence imaging system. The outcomes of our investigation indicate that the spleen acts as the primary organ for hematopoietic cell inflation. The spleen's role as a hematopoietic organ in humans under diverse pathological

conditions, including myelofibrosis, anemia, pregnancy, and inflammation, has been extensively documented.<sup>23–35</sup> Furthermore, splenic hematopoiesis following BM transplantation has been shown in humans through imaging studies utilizing 18F-fluorothymidine (18F-FLT), where temporal alterations in 18F-FLT uptake confirm cell proliferation in the spleen after HSC transplantation.<sup>36,37</sup> Recent advancements in single-cell RNA-seq (scRNA-seq) have further elucidated the specific hematopoietic systems within the human spleen, providing a deeper understanding of its role in human hematopoiesis.<sup>38</sup> These observations indicate that, similar to murine models, the human spleen facilitates a hematopoietic process distinct from that of the BM after HSC transplantation.

In murine studies, niche cells in the spleen, including endothelial cells, stromal cells, and macrophages that produce stem cell factor (SCF) and CXCL12, have been identified, indicating that the same hematopoietic regulatory mechanisms are present in both the BM and the spleen.<sup>39,40</sup> However, our findings suggest that the spleen plays a distinctive role in initiating hematopoietic cell inflation. Given that the BM fails to compensate for the loss of splenic hematopoiesis in splenectomized mice, it is plausible that the spleen orchestrates its own distinct regulatory mechanisms governing hematopoiesis. While the specific microenvironment responsible for spleen-specific hematopoiesis remains elusive, the observed alterations in Notch and Wnt signaling pathways within BM vascular endothelial cells under 5-fluorouracil (5-FU)-induced suppression suggest that exploring these pathways in the spleen could yield pivotal insights into the regulatory mechanisms driving post-transplant hematopoiesis in the spleen.<sup>41</sup>

Single-cell multiome analysis on CMP fractions revealed the emergence of CMP populations bearing a stem cell signature in exCMPs and SPaCMPs. Although infrequent, this population was also identified in fCMPs. The presence of a stem cell-like signature in progenitor cells suggests a hierarchy structure within the progenitor cell fraction, providing insights into a hematopoietic system driven by progenitor cells. Functional analysis following transplantation demonstrated that Hlf-High exCMPs induced markedly enhanced hematopoietic cell inflation in the spleen and generated a significantly greater number of cells compared to Hlf-Low exCMPs. This observation suggests that Hlf-High exCMPs possess superior self-renewal capacity compared to Hlf-Low exCMPs. However, their differentiation potential was restricted to the myeloid lineage, and they lacked the capacity for long-term BM reconstitution, a defining characteristic that distinguishes them from HSCs. Notably, HSC-specific genes such as *Hlf*, *Mecom*, and *Fgd5* were significantly upregulated in Hlf-High CMPs, suggesting potential biological similarities between Hlf-High CMPs and HSCs. However, the extent and nature of these similarities remain unclear, highlighting the need for further investigation to elucidate the functional and mechanistic implications of this gene expression overlap. The enrichment of CMPs with a stem cell-like signature in exCMPs likely plays a pivotal role in enhancing the progenitor effect, thereby driving robust hematopoietic cell inflation. While the precise mechanism underlying the enrichment of this population in exCMPs remains elusive, it is hypothesized that the selective serum-free culture method, targeting HSC expansion with high

concentration of thrombopoietin (TPO) and SCF, may contribute to this phenomenon. Further studies are needed to unravel the molecular and environmental factors that govern the emergence of Hlf-High exCMPs.

DPP4, a serine protease located on the cell surface, is recognized for its ability to alter protein function by cleaving particular amino acids at the N-terminal position. Its influence on the hematopoietic system has been extensively researched, and it is known to cleave CXCL12 in HSCs.<sup>42,43</sup> Scientists have explored the possibility of administering DPP4 inhibitors to promote HSC engraftment since the inhibition of DPP4 has been found to improve HSC homing to the BM.<sup>42,44</sup> In our study, we have discovered that reduced DPP4 activity is a mechanism by which exCMPs can initiate hematopoietic cell inflation earlier than fCMPs. In fact, exCMPs displayed a more acute response to G-CSF than fCMPs. Thus, while DPP4 activity affects HSC engraftment, we found it to have a significant impact on the formation of hematopoietic cell inflation in the spleen of early post-transplant recipients.

Rapid reconstitution of hematopoietic cells following HSC transplantation is crucial, as it mitigates the risk of infection and hemorrhage during the critical early post-transplantation period. While umbilical cord blood is a readily accessible source of HSCs for transplantation, it frequently contains an insufficient quantity of HSCs to ensure successful early hematopoietic reconstitution.<sup>45</sup> Hematopoietic recovery post cord blood transplantation often extends beyond 3 weeks, thereby prolonging cytopenia and increasing the risk of infections and bleeding complications. This challenge represents a substantial barrier to the broader and safer therapeutic application of cord blood HSCs. To overcome this limitation, a range of HSC expansion technologies is under development.<sup>16,17,46,47</sup> Although HSC expansion is essential, it alone does not suffice to guarantee early hematopoietic recovery following transplantation. By integrating HSC expansion technologies with solutions specifically targeting early hematopoietic recovery, such as our UNexCMPs, which leverage progenitor effects, cord blood could emerge as a more widely utilized and accessible stem cell source for a greater number of patients in need.

Moreover, exCMPs possess significant potential to meet clinical demands. In the clinical setting, numerous patients endure severe cytopenia due to disease progression or intense chemotherapy, complicating infection control and delaying eligibility for BM transplantation. For these patients, the temporary replenishment of neutrophils, macrophages, erythrocytes, and platelets via exCMPs may serve as a critical supportive therapy. Although prophylactic antibiotics are routinely administered to reduce infection risks during the post-transplant cytopenic phase, their prolonged use can perturb beneficial gut microbiota, thereby escalating the risk of infections and graft-versus-host disease (GVHD).<sup>48</sup> Our exCMPs may reduce the need for extended antibiotic use, thus preserving the integrity of gut microbiota. While granulocyte transfusion therapy effectively manages severe granulocytopenia,<sup>49</sup> it is limited by the challenge of securing large quantities of granulocytes. In contrast, exCMPs can be easily expanded *ex vivo*, producing large numbers of neutrophils and macrophages with a single administration, sustaining cell

populations for 1–2 weeks, and simultaneously replenishing erythrocytes and platelets, making them an invaluable post-transplant supportive therapy.

In our study, while exCMPs from C57BL/6NCr mice failed to induce hematopoiesis in the spleen of BALB/c mice, UNexCMPs successfully established hematopoietic cell inflation during allogeneic transplantation. This implies that the universalization of exCMPs can render the spleen available as a hematopoietic tissue rather than an immune tissue. Consequently, UNexCMPs may facilitate early hematopoiesis in humans even in allogeneic settings,<sup>50</sup> utilizing the spleen as a hematopoietic site. In this study, we created the UNexCMPs through MHC class I knockout and designed them to function effectively but transiently following preconditioning treatments such as radiation prior to BM transplantation. Considering the radiation sensitivity of human NK cells,<sup>51</sup> we hypothesize that NK activity is diminished post -radiation, making universal exCMPs feasible in such scenarios. However, to fully optimize universal cells, strategies to evade NK cell-mediated attacks are imperative. Recent advancements in cell universalization, including the development of pseudo-homozygous HLA cells and HLA-C-retained cells,<sup>52</sup> have successfully circumvented NK cell-mediated allo-rejection. These developments offer valuable insights for improving our exCMPs, which are readily cultured and genome edited, facilitating the creation of more sophisticated universal cells.

In our study, we reinterpreted the colony-forming unit assay from the 1960s using cutting-edge technologies and introduced the concept of hematopoietic cell inflation. We thoroughly analyzed the spatiotemporal dynamics of post-transplant hematopoiesis, leading to the development of exCMPs. Supportive therapies using UNexCMPs can be administered in all situations beyond the allogeneic barrier and have the potential to become off-the-shelf cellular products that can address the need for early hematopoietic recovery after transplantation and chemotherapy in real-world clinical practice. We hope that the findings of this study will serve as a steppingstone toward widespread clinical application.

### Limitations of the study

This study employed murine models to conduct human exCMP transplantation experiments. However, the microenvironment of the murine BM and spleen differs from that of humans, and the interaction between the transplanted human blood cells and the microenvironment may not be optimal. Therefore, without actual administration into the human body, it cannot be confirmed whether human exCMPs can support hematopoiesis in the human spleen. Nonetheless, several previous reports have demonstrated the spleen's hematopoietic potential in humans, suggesting that human exCMPs may facilitate early hematopoiesis in the human spleen. While our findings offer important insights into this possibility, extrapolation to human clinical scenarios requires caution due to interspecies differences in spleen physiology and hematopoietic dynamics. Elucidating the specific micro-environment that supports hematopoietic cell inflation driven by exCMPs in the murine spleen and exploring whether analogous cells or structures are present in the human spleen

represent critical next steps. Additionally, future investigations employing non-human primate models will be crucial to confirm the translatability of these results to human systems.

### RESOURCE AVAILABILITY

#### Lead contact

Further information and requests for resources and reagents should be directed to Satoshi Yamazaki ([y-sato4@ims.u-tokyo.ac.jp](mailto:y-sato4@ims.u-tokyo.ac.jp)).

#### Materials availability

This study did not generate new unique reagents.

#### Data and code availability

- The bulk RNA-seq and scMultiome data have been deposited in the GEO under the accession codes GSE: 285275 (bulk) and GSE: 285278 (scMultiome). Source data have been uploaded to Mendeley Data (<https://doi.org/10.17632/3ttmmmhkm3.1>). Further information and requests for resources and reagents should be directed to and will be fulfilled by the [lead contact](#).
- This paper does not report original code.
- Any additional information required to reanalyze the data reported in this paper is available from the [lead contact](#) upon request.

### ACKNOWLEDGMENTS

We thank the University of Tokyo Institute of Medical Science (IMSUT) FACS core laboratory for technical assistance. We thank Dr. M. Muratani and Tsukuba i-Laboratory LLP for sequencing services. This work was supported by the Japan Society for the Promotion of Science (JSPS; #21F21108 and #20K21612 to S.Y., #24K19192 to T.Y., and #23K15315 to H.J.B.) and the Japan Agency for Medical Research and Development (AMED; #21bm0404077h0001, #21bm0704055h0002, and #23bm1223011h0001 to S.Y.).

### AUTHOR CONTRIBUTIONS

Conceptualization, T. Yogo and S.Y.; methodology, T. Yogo, H.J.B., S.I., T. Kuchimaru, T. Kimura, A.M., T. Yokomizo, S.T., A.I., and S.Y.; investigation, T. Yogo; analysis, T. Yogo and T. Kimura; writing T. Yogo; funding acquisition, S.Y., T. Yogo, and H.J.B.; supervision, S.Y.

### DECLARATION OF INTERESTS

The authors have no relevant interests to disclose.

### STAR METHODS

Detailed methods are provided in the online version of this paper and include the following:

- KEY RESOURCES TABLE**
- EXPERIMENTAL MODEL AND SUBJECT DETAILS**
  - Mice
  - Murine and human HSPC culture
- METHOD DETAILS**
  - Murine HSC isolation
  - Akaluc bone marrow chimeric mice
  - CRISPR/Cas9 gene editing
  - Peripheral blood analysis
  - Akaluc vector transduction
  - Cell counting and sample preparation for flow cytometry
  - In vivo* luminescence imaging
  - RNAseq analysis
  - Single-cell multiome analysis
  - Transplantation assay

- DPP4 activity assay
- *In vivo* G-CSF reactivity assay
- QUANTIFICATION AND STATISTICAL ANALYSIS

#### SUPPLEMENTAL INFORMATION

Supplemental information can be found online at <https://doi.org/10.1016/j.celrep.2025.115241>.

Received: August 18, 2024

Revised: October 22, 2024

Accepted: January 7, 2025

Published: January 25, 2025

#### REFERENCES

1. Laurenti, E., and Göttgens, B. (2018). From haematopoietic stem cells to complex differentiation landscapes. *Nature* **553**, 418–426. <https://doi.org/10.1038/nature25022>.
2. Chabannon, C., Kuball, J., Bondanza, A., Dazzi, F., Pedrazzoli, P., Toubert, A., Ruggeri, A., Fleischhauer, K., and Bonini, C. (2018). Hematopoietic stem cell transplantation in its 60s: A platform for cellular therapies. *Sci. Transl. Med.* **10**, 9630. <https://doi.org/10.1126/scitranslmed.aap9630>.
3. Yamazaki, S., Ema, H., Karlsson, G., Yamaguchi, T., Miyoshi, H., Shioda, S., Taketo, M.M., Karlsson, S., Iwama, A., and Nakuchi, H. (2011). Non-myelinating Schwann Cells Maintain Hematopoietic Stem Cell Hibernation in the Bone Marrow Niche. *Cell* **147**, 1146–1158. <https://doi.org/10.1016/J.CELL.2011.09.053>.
4. Taya, Y., Ota, Y., Wilkinson, A.C., Kanazawa, A., Watarai, H., Kasai, M., Nakuchi, H., and Yamazaki, S. (2016). Depleting dietary valine permits nonmyeloablative mouse hematopoietic stem cell transplantation. *Science* **354**, 1152–1155. <https://doi.org/10.1126/SCIENCE.AAG3145>.
5. Till, J.E., and McCulloch, E.A. (1961). A direct measurement of the radiation sensitivity of normal mouse bone marrow cells. *Radiat. Res.* **14**, 213–222. <https://doi.org/10.2307/3570892>.
6. Magli, M.C., Iscove, N.N., and Odartchenko, N. (1982). Transient nature of early haematopoietic spleen colonies. *Nature* **295**, 527–529. <https://doi.org/10.1038/295527a0>.
7. Iwano, S., Sugiyama, M., Hama, H., Watakabe, A., Hasegawa, N., Kuchimaru, T., Tanaka, K.Z., Takahashi, M., Ishida, Y., Hata, J., et al. (2018). Single-cell bioluminescence imaging of deep tissue in freely moving animals. *Science* **359**, 935–939. <https://doi.org/10.1126/science.aaq1067>.
8. Thomas, E.D., Lochte, H.L., Jr., Lu, W.C., and Ferrebee, J.W. (1957). Intra-venous Infusion of Bone Marrow in Patients Receiving Radiation and Chemotherapy. *N. Engl. J. Med.* **257**, 491–496. <https://doi.org/10.1056/NEJM195709122571102>.
9. Ruggeri, A., Labopin, M., Sormani, M.P., Sanz, G., Sanz, J., Volt, F., Michel, G., Locatelli, F., Diaz De Heredia, C., O'Brien, T., et al. (2014). Engraftment kinetics and graft failure after single umbilical cord blood transplantation using a myeloablative conditioning regimen. *Haematologica* **99**, 1509–1515. <https://doi.org/10.3324/haematol.2014.109280>.
10. Schmitz, N., Beksac, M., Hasenclever, D., Bacigalupo, A., Ruutu, T., Nagerl, A., Gluckman, E., Russell, N., Apperley, J.F., Gorin, N.C., et al. (2002). Transplantation of mobilized peripheral blood cells to HLA-identical siblings with standard-risk leukemia. *Blood* **100**, 761–767. <https://doi.org/10.1182/BLOOD-2001-12-0304>.
11. Mandal, P.K., Ferreira, L.M.R., Collins, R., Meissner, T.B., Boutwell, C.L., Friesen, M., Vrbanac, V., Garrison, B.S., Stortchevoi, A., Bryder, D., et al. (2014). Efficient ablation of genes in human hematopoietic stem and effector cells using CRISPR/Cas9. *Cell Stem Cell* **15**, 643–652. <https://doi.org/10.1016/j.stem.2014.10.004>.
12. Riolobos, L., Hirata, R.K., Turtle, C.J., Wang, P.R., Gornalusse, G.G., Zavajlevski, M., Riddell, S.R., and Russell, D.W. (2013). HLA engineering of human pluripotent stem cells. *Mol. Ther.* **21**, 1232–1241. <https://doi.org/10.1038/mt.2013.59>.
13. Ichise, H., Nagano, S., Maeda, T., Miyazaki, M., Miyazaki, Y., Kojima, H., Yawata, N., Yawata, M., Tanaka, H., Saji, H., et al. (2017). NK Cell Alloreactivity against KIR-Ligand-Mismatched HLA-Haploididentical Tissue Derived from HLA Haplotype-Homozygous iPSCs. *Stem Cell Rep.* **9**, 853–867. <https://doi.org/10.1016/j.stemcr.2017.07.020>.
14. Gornalusse, G.G., Hirata, R.K., Funk, S.E., Riolobos, L., Lopes, V.S., Manske, G., Prunkard, D., Colunga, A.G., Hanafi, L.A., Clegg, D.O., et al. (2017). HLA-E-expressing pluripotent stem cells escape allogeneic responses and lysis by NK cells. *Nat. Biotechnol.* **35**, 765–772. <https://doi.org/10.1038/nbt.3860>.
15. Wilkinson, A.C., Ishida, R., Kikuchi, M., Sudo, K., Morita, M., Crisostomo, R.V., Yamamoto, R., Loh, K.M., Nakamura, Y., Watanabe, M., et al. (2019). Long-term ex vivo haematopoietic-stem-cell expansion allows nonconditioned transplantation. *Nature* **571**, 117–121. <https://doi.org/10.1038/s41586-019-1244-x>.
16. Boitano, A.E., Wang, J., Romeo, R., Bouchez, L.C., Parker, A.E., Sutton, S.E., Walker, J.R., Flaveny, C.A., Perdew, G.H., Denison, M.S., et al. (2010). Aryl hydrocarbon receptor antagonists promote the expansion of human hematopoietic stem cells. *Science* **329**, 1345–1348. <https://doi.org/10.1126/SCIENCE.1191536>.
17. Fares, I., Chagraoui, J., Gareau, Y., Gingras, S., Ruel, R., Mayotte, N., Csaszar, E., Knapp, D.J.H.F., Miller, P., Ngom, M., et al. (2014). Pyrimidoindole derivatives are agonists of human hematopoietic stem cell self-renewal. *Science* **345**, 1509–1512. <https://doi.org/10.1126/SCIENCE.1256337>.
18. Broxmeyer, H.E., Hoggatt, J., O'leary, H.A., Mantel, C., Chitteti, B.R., Cooper, S., Messina-Graham, S., Hangoc, G., Farag, S., Rohrbaugh, S.L., et al. (2012). Dipeptidylpeptidase 4 negatively regulates colony-stimulating factor activity and stress hematopoiesis. *Nat. Med.* **18**, 1786–1796. <https://doi.org/10.1038/nm.2991>.
19. Paul, F., Arkin, Y., Giladi, A., Jaitin, D.A., Kenigsberg, E., Keren-Shaul, H., Winter, D., Lara-Astiaso, D., Gury, M., Weiner, A., et al. (2015). Transcriptional Heterogeneity and Lineage Commitment in Myeloid Progenitors. *Cell* **163**, 1663–1677. <https://doi.org/10.1016/j.cell.2015.11.013>.
20. Kim, S., Lin, L., Brown, G.A.J., Hosaka, K., and Scott, E.W. (2017). Extended time-lapse *in vivo* imaging of tibia bone marrow to visualize dynamic hematopoietic stem cell engraftment. *Leukemia* **31**, 1582–1592. <https://doi.org/10.1038/leu.2016.354>.
21. Cao, Y.-A., Wagers, A.J., Beilhack, A., Dusich, J., Bachmann, M.H., Neigrin, R.S., Weissman, I.L., and Contag, C.H. (2004). Shifting foci of hematopoiesis during reconstitution from single stem cells. *Proc. Natl. Acad. Sci. USA* **101**, 221–226. <https://doi.org/10.1073/pnas.2637010100>.
22. Wang, X., Rosol, M., Ge, S., Peterson, D., McNamara, G., Pollack, H., Kohn, D.B., Nelson, M.D., and Crooks, G.M. (2003). Dynamic tracking of human hematopoietic stem cell engraftment using *in vivo* bioluminescence imaging. *Blood* **102**, 3478–3482. <https://doi.org/10.1182/blood-2003-05-1432>.
23. Yamamoto, K., Miwa, Y., Abe-Suzuki, S., Abe, S., Kirimura, S., Onishi, I., Kitagawa, M., and Kurata, M. (2016). Extramedullary hematopoiesis: Elucidating the function of the hematopoietic stem cell niche (Review). *Mol. Med. Rep.* **13**, 587–591. <https://doi.org/10.3892/mmr.2015.4621>.
24. Mende, N., and Laurenti, E. (2021). Hematopoietic stem and progenitor cells outside the bone marrow: where, when, and why. *Exp. Hematol.* **104**, 9–16. <https://doi.org/10.1016/j.exphem.2021.10.002>.
25. Roberts, A.S., Shetty, A.S., Mellnick, V.M., Pickhardt, P.J., Bhalla, S., and Menias, C.O. (2016). Extramedullary haematopoiesis: radiological imaging features. *Clin. Radiol.* **71**, 807–814. <https://doi.org/10.1016/j.crad.2016.05.014>.
26. Karimi, M., Bagheri, M.H., Tahmtan, M., Shakibafard, A., and Rashid, M. (2009). Prevalence of hepatosplenomegaly in beta thalassemia minor subjects in Iran. *Eur. J. Radiol.* **69**, 120–122. <https://doi.org/10.1016/j.ejrad.2007.09.027>.

27. Maymon, R., Strauss, S., Vaknin, Z., Weinraub, Z., Herman, A., and Gayer, G. (2006). Normal sonographic values of maternal spleen size throughout pregnancy. *Ultrasound Med. Biol.* 32, 1827–1831. <https://doi.org/10.1016/j.ultrasmedbio.2006.06.017>.
28. Sheehan, H.L., and Falkiner, N.M. (1948). Splenic Aneurysm and Splenic Enlargement in Pregnancy. *Br. Med. J.* 2, 1105. <https://doi.org/10.1136/BMJ.2.4590.1105>.
29. Emami, H., Singh, P., Macnabb, M., Vucic, E., Lavender, Z., Rudd, J.H.F., Fayad, Z.A., Lehrer-Graiwer, J., Korsgren, M., Figueroa, A.L., et al. (2015). Splenic Metabolic Activity Predicts Risk of Future Cardiovascular Events: Demonstration of a Cardiosplenic Axis in Humans. *JACC. Cardiovasc. Imaging* 8, 121–130. <https://doi.org/10.1016/J.JCMG.2014.10.009>.
30. Wu, C., Ning, H., Liu, M., Lin, J., Luo, S., Zhu, W., Xu, J., Wu, W.C., Liang, J., Shao, C.K., et al. (2018). Spleen mediates a distinct hematopoietic progenitor response supporting tumor-promoting myelopoiesis. *J. Clin. Invest.* 128, 3425–3438. <https://doi.org/10.1172/JCI97973>.
31. Ojeda-Uribe, M., Morel, O., Ungureanu, C., Desterke, C., Le Bousse-Kerdiès, M.C., and Bouladour, H. (2016). Assessment of sites of marrow and extramedullary hematopoiesis by hybrid imaging in primary myelofibrosis patients. *Cancer Med.* 5, 2378–2384. <https://doi.org/10.1002/CAM4.835>.
32. Wang, X., Prakash, S., Lu, M., Tripodi, J., Ye, F., Najfeld, V., Li, Y., Schwartz, M., Weinberg, R., Roda, P., et al. (2012). Spleens of myelofibrosis patients contain malignant hematopoietic stem cells. *J. Clin. Invest.* 122, 3888–3899. <https://doi.org/10.1172/JCI64397>.
33. Barosi, G., Viarengo, G., Pecci, A., Rosti, V., Piaggio, G., Marchetti, M., and Frassoni, F. (2001). Diagnostic and clinical relevance of the number of circulating CD34+ cells in myelofibrosis with myeloid metaplasia. *Blood* 98, 3249–3255. <https://doi.org/10.1182/BLOOD.V98.12.3249>.
34. Mesa, R.A., Li, C.Y., Schroeder, G., and Tefferi, A. (2001). Clinical correlates of splenic histopathology and splenic karyotype in myelofibrosis with myeloid metaplasia. *Blood* 97, 3665–3667. <https://doi.org/10.1182/BLOOD.V97.11.3665>.
35. Bacigalupo, A., Soraru, M., Dominietto, A., Pozzi, S., Geroldi, S., Van Lint, M.T., Ibatici, A., Raiola, A.M., Frassoni, F., De Stefano, F., et al. (2010). Allogeneic hematopoietic SCT for patients with primary myelofibrosis: a predictive transplant score based on transfusion requirement, spleen size and donor type. *Bone Marrow Transplant.* 45, 458–463. <https://doi.org/10.1038/bmt.2009.188>.
36. Williams, K.M., Holter-Chakrabarty, J., Lindenberg, L., Duong, Q., Vesely, S.K., Nguyen, C.T., Havlicek, J.P., Kurdziel, K., Gea-Banacloche, J., Lin, F.I., et al. (2018). Imaging of subclinical haemopoiesis after stem-cell transplantation in patients with haematological malignancies: a prospective pilot study. *Lancet Haematol.* 5, e44–e52. [https://doi.org/10.1016/S2352-3026\(17\)30215-6](https://doi.org/10.1016/S2352-3026(17)30215-6).
37. Williams, K.M., and Chakrabarty, J.H. (2020). Imaging haemopoietic stem cells and microenvironment dynamics through transplantation. *Lancet Haematol.* 7, e259–e269. [https://doi.org/10.1016/S2352-3026\(20\)30003-X](https://doi.org/10.1016/S2352-3026(20)30003-X).
38. Mende, N., Bastos, H.P., Santoro, A., Mahbubani, K.T., Ciaurro, V., Calderbank, E.F., Quiroga Londoño, M., Sham, K., Mantica, G., Morishima, T., et al. (2022). Unique molecular and functional features of extramedullary hematopoietic stem and progenitor cell reservoirs in humans. *Blood* 139, 3387–3401. <https://doi.org/10.1182/BLOOD.2021013450>.
39. Inra, C.N., Zhou, B.O., Acar, M., Murphy, M.M., Richardson, J., Zhao, Z., and Morrison, S.J. (2015). A perisinusoidal niche for extramedullary haematopoiesis in the spleen. *Nature* 527, 466–471. <https://doi.org/10.1038/nature15530>.
40. Chen, Y., Xiang, J., Qian, F., Diwakar, B.T., Ruan, B., Hao, S., Prabhu, K.S., and Paulson, R.F. (2020). Epo receptor signaling in macrophages alters the splenic niche to promote erythroid differentiation. *Blood* 136, 235–246. <https://doi.org/10.1182/blood.2019003480>.
41. Tikhonova, A.N., Dolgalev, I., Hu, H., Sivaraj, K.K., Hoxha, E., Cuesta-Domínguez, Á., Pinho, S., Akhmetzyanova, I., Gao, J., Witkowski, M., et al. (2019). The bone marrow microenvironment at single-cell resolution. *Nature* 569, 222–228. <https://doi.org/10.1038/s41586-019-1104-8>.
42. Christopherson, K.W., Hangoc, G., Mantel, C.R., and Broxmeyer, H.E. (2004). Modulation of Hematopoietic Stem Cell Homing and Engraftment by CD26. *Science* 305, 1000–1003. <https://doi.org/10.1126/SCIENCE.1097071>.
43. Christopherson, K.W., Cooper, S., and Broxmeyer, H.E. (2003). Cell surface peptidase CD26/DPPIV mediates G-CSF mobilization of mouse progenitor cells. *Blood* 101, 4680–4686. <https://doi.org/10.1182/BLOOD-2002-12-3893>.
44. Farag, S.S., Srivastava, S., Messina-Graham, S., Schwartz, J., Robertson, M.J., Abonour, R., Cornetta, K., Wood, L., Secret, A., Strother, R.M., et al. (2013). In Vivo DPP-4 Inhibition to Enhance Engraftment of Single-Unit Cord Blood Transplants in Adults with Hematological Malignancies. *Stem Cell. Dev.* 22, 1007–1015. <https://doi.org/10.1089/SCD.2012.0636>.
45. Pineault, N., and Abu-Khader, A. (2015). Advances in umbilical cord blood stem cell expansion and clinical translation. *Exp. Hematol.* 43, 498–513. <https://doi.org/10.1016/J.EXPHEM.2015.04.011>.
46. Sakurai, M., Ishitsuka, K., Ito, R., Wilkinson, A.C., Kimura, T., Mizutani, E., Nishikii, H., Sudo, K., Becker, H.J., Takemoto, H., et al. (2023). Chemically defined cytokine-free expansion of human haematopoietic stem cells. *Nature (London, U. K.)* 615, 127–133. <https://doi.org/10.1038/s41586-023-05739-9>.
47. Meaker, G.A., and Wilkinson, A.C. (2024). Ex vivo hematopoietic stem cell expansion technologies: recent progress, applications, and open questions. *Exp. Hematol.* 130, 104136. <https://doi.org/10.1016/J.EXPHEM.2023.12.001>.
48. Taur, Y., Coyte, K., Schluter, J., Robilotti, E., Figueroa, C., Gjonbalaj, M., Littmann, E.R., Ling, L., Miller, L., Gyaltschen, Y., et al. (2018). Reconstitution of the gut microbiota of antibiotic-treated patients by autologous fecal microbiota transplant. *Sci. Transl. Med.* 10, eaap9489. <https://doi.org/10.1126/SCITRANSLMED.AAP9489>.
49. Price, T.H., Boeckh, M., Harrison, R.W., McCullough, J., Ness, P.M., Strauss, R.G., Nichols, W.G., Hamza, T.H., Cushing, M.M., King, K.E., et al. (2015). Efficacy of transfusion with granulocytes from G-CSF/dexamethasone-treated donors in neutropenic patients with infection. *Blood* 126, 2153–2161. <https://doi.org/10.1182/BLOOD-2015-05-645986>.
50. Akpek, G., Pasquini, M.C., Logan, B., Agovi, M.-A., Lazarus, H.M., Marks, D.I., Bornhaeuser, M., Ringdén, O., Maziarz, R.T., Gupta, V., et al. (2013). Effects of spleen status on early outcomes after hematopoietic cell transplantation. *Bone Marrow Transplant.* 48, 825–831. <https://doi.org/10.1038/bmt.2012.249>.
51. Seki, H., Iwai, K., Kanegae, H., Konno, A., Ohta, K., Ohta, K., Yachie, A., Taniguchi, N., and Miyawaki, T. (1995). Differential Protective Action of Cytokines on Radiation-Induced Apoptosis of Peripheral Lymphocyte Subpopulations. *Cell. Immunol.* 163, 30–36. <https://doi.org/10.1006/CIMM.1995.1095>.
52. Xu, H., Wang, B., Ono, M., Kagita, A., Fujii, K., Sasakawa, N., Ueda, T., Gee, P., Nishikawa, M., Nomura, M., et al. (2019). Targeted Disruption of HLA Genes via CRISPR-Cas9 Generates iPSCs with Enhanced Immune Compatibility. *Cell Stem Cell* 24, 566–578.e7. <https://doi.org/10.1016/j.stem.2019.02.005>.
53. Becker, H.J., Ishida, R., Wilkinson, A.C., Kimura, T., Lee, M.S.J., Coban, C., Ota, Y., Tanaka, Y., Roskamp, M., Sano, T., et al. (2023). Controlling genetic heterogeneity in gene-edited hematopoietic stem cells by single-cell expansion. *Cell Stem Cell* 30, 987–1000.e8. <https://doi.org/10.1016/j.stem.2023.06.002>.

## STAR★METHODS

### KEY RESOURCES TABLE

REAGENT or RESOURCE	SOURCE	IDENTIFIER
<b>Antibodies</b>		
anti-mouse cKit-APC (2B8)	Thermo Fisher Scientific	Cat#17-1171-83; RRID:AB_469431
anti-mouse CD4-APC (RM4-5)	Thermo Fisher Scientific	Cat#17-0042-83; RRID:AB_469324
anti-mouse CD8a-APC (53-6.7)	Thermo Fisher Scientific	Cat#17-0081-83; RRID:AB_469336
anti-mouse CD45.1-APC/Cy7 (A20)	Tonbo Biosciences	Cat#25-0453; RRID:AB_2621629
anti-mouse Sca-1-APC/Cy7 (D7)	BioLegend	Cat#108126; RRID:AB_10645327
anti-mouse CD45R(B220)-APC/eFluor780 (RA3-6B2)	Thermo Fisher Scientific	Cat#47-0452-82; RRID:AB_1518810
anti-mouse Ckit-APC/H7 (2B8)	BD Biosciences	Cat#560185; RRID:AB_1645231
anti-mouse CD4-Biotin (RM4-5)	Thermo Fisher Scientific	Cat#13-0042-85; RRID:AB_466330
anti-mouse CD8a-Biotin (53-6.7)	Thermo Fisher Scientific	Cat#13-0081-85; RRID:AB_466347
anti-mouse CD45R(B220)-Biotin (RA3-6B2)	Thermo Fisher Scientific	Cat#13-0452-82; RRID:AB_466449
anti-mouse TER119-Biotin (TER119)	Thermo Fisher Scientific	Cat#13-5921-85; RRID:AB_466798
anti-mouse Gr1-Biotin (RB6-8C5)	Thermo Fisher Scientific	Cat#13-5931-85-85; RRID:AB_466801
anti-mouse CD11b-Biotin (M1/70)	Thermo Fisher Scientific	Cat#13-0112-85; RRID:AB_466360
anti-mouse CD127-Biotin (A7R34)	Thermo Fisher Scientific	Cat#13-1271-85; RRID:AB_466589
anti-mouse CD45.2-BV421 (104)	Thermo Fisher Scientific	Cat#48-0454-82; RRID:AB_11042125
anti-mouse CD41-BV510 (MWReg30)	BioLegend	Cat#133923; RRID: AB_2739892
anti-mouse Sca-1-BV605 (D7)	BioLegend	Cat#108133; RRID: AB_2562275
anti-mouse CD105-BV786 (MJ7/18)	BD Biosciences	Cat#564746; RRID: AB_2732065
anti-mouse MHC Class II- eFluor™ 450 (M5/114.15.2)	Thermo Fisher Scientific	Cat# 48-5321-82; RRID: AB_1272204
anti-mouse CD34-FITC (RAM34)	Thermo Fisher Scientific	Cat#11-0341-85; RRID:AB_465022
anti-mouse CD4-PB (RM4-5)	BioLegend	Cat#100531; RRID:AB_493374
anti-mouse CD8a-PB (53-6.7)	BD Biosciences	Cat#558106; RRID:AB_397029
anti-mouse CD34-PB (RAM34)	BioLegend	Cat# 11-0341-85; RRID: AB_465021
anti-mouse CD45R(B220)-PB (RA3-6B2)	BD Biosciences	Cat#558108; RRID:AB_397031
anti-mouse TER119-PB (TER119)	BioLegend	Cat#116231; RRID:AB_2149212
anti-mouse Gr1-PB (RB6-8C5)	BioLegend	Cat#108430; RRID:AB_893556
anti-mouse CD11b-PB (M1/70)	BioLegend	Cat#101224; RRID:AB_755986
anti-mouse Sca-1-PE (D7)	Thermo Fisher Scientific	Cat#12-5981-83; RRID:AB_466087
anti-mouse CD201-PE (eBio1560)	Thermo Fisher Scientific	Cat#12-2012-82; RRID:AB_914317
anti-mouse Gr1-PE (RB6-8C5)	Thermo Fisher Scientific	Cat#12-5931-83; RRID:AB_466046
anti-mouse CD11b-PE (M1/70)	BD Biosciences	Cat#557397; RRID:AB_396680
anti-mouse CD150-PE/Cy7 (TC15-12F12.2)	BioLegend	Cat#115913; RRID:AB_439796
anti-mouse CD16/32-PE/Cy7(93)	BioLegend	Cat#101318; RRID: AB_2104156
anti-mouse CD45.1-PE/Cy7 (A20)	Tonbo Biosciences	Cat#60-0453; RRID:AB_2621850
anti-mouse CD8a-PE/Cy7 (53-6.7)	BioLegend	Cat#100722; RRID:AB_312761
Streptavidin-APC/eFluor780	Thermo Fisher Scientific	Cat#47-4317-82; RRID:AB_10366688
Streptavidin-BV421	BioLegend	Cat#405225; RRID:AB_3662382
anti-human CD34-APC (581)	BioLegend	Cat#343510; RRID:AB_1877153
anti-human CD33-PE/Cy7 (WM53)	Thermo Fisher Scientific	Cat#25-0338-42; RRID:AB_1907380
anti-human CD45RA-APC/Cy7 (HI100)	BioLegend	Cat# 304128; RRID: AB_10708880
anti-human CD123-PE (6H6)	BioLegend	Cat# 306006; RRID: AB_314580
anti-human HLA-A,B,C-PB	BioLegend	Cat# 311418; RRID: AB_493669

(Continued on next page)

**Continued**

REAGENT or RESOURCE	SOURCE	IDENTIFIER
anti-human CD45-APC/Cy7 (HI30)	BioLegend	Cat#304014; RRID:AB_314402
anti-mouse CD45.1-eFluor 450 (A20)	Thermo Fisher Scientific	Cat#48-0453-82; RRID:AB_1272189
<b>Biological samples</b>		
Human CD34 <sup>+</sup> cord blood HSCs	StemExpress	Cat#CB3400.5C
<b>Chemicals, peptides, and recombinant proteins</b>		
Polyvinyl alcohol (PVA), 87–90% hydrolyzed	Sigma	Cat#P8136; CAS 9002-89-5
Recombinant Murine TPO	Peprotech	Cat#315-14; P40226
Recombinant Murine SCF	Peprotech	Cat#250-03; P20826
Insulin-Transferrin-Selenium	Thermo Fisher Scientific	Cat#41400045
<b>Deposited data</b>		
Raw figure data	This paper	Mendeley Data: <a href="https://doi.org/10.17632/3ttmmmhkm3.1">https://doi.org/10.17632/3ttmmmhkm3.1</a>
BulkRNASeq	This paper	GEO: GSE285275
scMultiome	This paper	GEO: GSE285278
<b>Experimental models: Organisms/strains</b>		
Mouse: CD45.2 + C57BL/6: C57BL/6NCrSlc	SLC	RRID:MGI:5295404
Mouse: CD45.1 + C57BL/6: B6.SJL-Ptprca Pepcb/BoyJ	Sankyo Labo	RRID:IMSR_JAX:002014
<b>Oligonucleotides</b>		
	See <a href="#">Tables S1</a> and <a href="#">S2</a> for list of oligonucleotides	N/A
<b>Software and algorithms</b>		
FlowJo version 10	BD	<a href="https://www.flowjo.com">https://www.flowjo.com</a> ; SCR_008520
Prism version 9.1	Graphpad	<a href="https://www.graphpad.com">https://www.graphpad.com</a> ; SCR_002798
R version 4.0.0	R Foundation	<a href="https://www.r-project.org">https://www.r-project.org</a> ; SCR_001905

## EXPERIMENTAL MODEL AND SUBJECT DETAILS

### Mice

C57BL/6NCrSlc (Ly 5.2, CD45.2) mice were purchased from SLC Inc., Japan, while C57BL/6-Ly5.1 (Ly5.1, CD45.1) mice were obtained from Sankyo Labo, Japan. The NOG mice were developed at the Central Institute for Experimental Animals. Hif-tdTomato mice were kindly provided by Tomomasa Yokomizo (Department of Microscopic and Developmental Anatomy, Tokyo Women's Medical University, Tokyo, Japan.). All mice were obtained at the age of 8–10 weeks and maintained in a specific-pathogen-free environment with free access to food and water. All animal studies were conducted in accordance with institutional protocols and were approved by the Animal Care and Use Committee of the Institute of Medical Science at the University of Tokyo and the Laboratory Animal Resource Center at the University of Tsukuba.

### Murine and human HSPC culture

Murine hematopoietic stem cells (HSCs) were cultured in Ham's F12 medium (Wako), enriched with 10 mM HEPES (Thermo Fisher Scientific), recombinant cytokines murine TPO (100 ng/mL, Peprotech), and SCF (10 ng/mL, Peprotech), polyvinyl alcohol (PVA, 84% hydrolyzed, Sigma), as well as insulin-transferrin-selenium (ITS, Thermo Fisher Scientific, 1:100 dilution) and 1% Penicillin-Streptomycin-L-Glutamine (PSG, Wako). Murine HSCs were cultured on untreated U-bottom 96-well plates (TPP, for cultures starting with 100 cells) or 24-well dishes (Corning, for cultures starting with 1000–3000 cells).

Human umbilical-cord-blood-derived CD34<sup>+</sup> cells were obtained from StemExpress (Folsom). For SR-1-based human HSC culture, CD34<sup>+</sup> cells were cultured in StemSpanSFEM (Stemcell Technologies) enriched with recombinant human SCF (50 ng/mL, PeproTech), FMS-like tyrosine kinase 3 ligand (FLT3, 50 ng/mL, PeproTech), human THPO (50 ng/mL, PeproTech), human Interleukin (IL) 6 (50 ng/mL, PeproTech), 1% PSG (Wako), and SR-1 (1 μM). For Nicotinamide-based human HSC culture, CD34<sup>+</sup> cells were cultured in MEMα (Wako) enriched with 10% FBS (PEAK), recombinant human SCF (50 ng/mL, PeproTech), FMS-like tyrosine kinase 3 ligand (FLT3, 50 ng/mL, PeproTech), human THPO (50 ng/mL, PeproTech), human IL6 (50 ng/mL, PeproTech), 1% PSG (Wako), and Nicotinamide (2.5 mM, Wako). Human CD34<sup>+</sup> cells were cultured on 24-well flat-bottomed CellBIND tissue culture

plates (Corning). Cells were maintained in an incubator (Panasonic) at 37°C with a constant CO<sub>2</sub> fraction of 5%, and medium changes were carried out every 2–3 days.

## METHOD DETAILS

### Murine HSC isolation

Male 9–10 week old male C57BL/6-CD45.1 mice were humanely sacrificed under isoflurane anesthesia. Pelvic, femur, and tibia bones were excised and crushed, and the resulting cell solution was filtered and the whole bone marrow cells were enumerated. Positive selection of cKit<sup>+</sup> cells was accomplished using anti-APC magnetic-activated cell sorting (MACS, Miltenyi Biotec) antibodies after staining the cells with cKit-APC antibody for 30 min. Enriched cKit<sup>+</sup> cells were then incubated with an anti-Lineage antibody cocktail (including biotinylated Gr1[LY-6G/LY-6C], CD11b, CD4, CD8a, CD45R[B220], IL7-R, TER119) for an additional 30 min. This was followed by a 90-min incubation with CD34-FITC, Sca1-PE, cKit-APC, streptavidin-APC/eFluor, and CD150-PE/Cy7 antibodies. Propidium iodide (PI) was employed to exclude dead cells. CD34<sup>−</sup>CD150<sup>+</sup>cKit<sup>+</sup>Sca1<sup>+</sup>Lin<sup>−</sup> (CD34<sup>−</sup>CD150<sup>+</sup>KSL) cells were sorted via fluorescence-activated cell sorting (FACS) on an Aria III cell sorter (BD) using a 100 µm nozzle and appropriate filters and settings.

### Akaluc bone marrow chimeric mice

Lentiviral vectors were utilized to transduce murine HSCs with the Akaluc gene. 10,000 Akaluc<sup>+</sup>CD201<sup>+</sup>CD150<sup>+</sup>KSL cells were mixed with 1.0x10<sup>5</sup> Sca1(−) bone marrow cells and transplanted into irradiated mice. Experiments were performed using bone marrow cells obtained from mice with 80–100% chimerism 16 or more weeks after transplantation.

### CRISPR/Cas9 gene editing

Gene editing for HSCs were performed as described previously.<sup>53</sup> Recombinant *S. pyogenes* Cas9 (S.p. Cas9 Nuclease V3, IDT) was complexed with single guide RNA (sgRNA, synthesized at IDT) at a molar ratio of 1:2.5 for 10 min at 25°C to form ribonucleoprotein (RNP) complexes. Sequences of sgRNA targeting murine Cxcr4, murine Itga4, murine B2m, and human B2M are listed in Table S1. HSCs were expanded and washed twice with PBS, pelleted, and resuspended in 20 µl electroporation buffer P3 (Lonza). The RNP duplex was gently added to the cells, and the suspension was transferred to a single 20 µl electroporation cuvette on a 16 well strip (P3 Primary Cell 96-well-Nucleofector Kit, Lonza). Electroporation was conducted using programs EO-100 on a 4D nucleofector device (Lonza). Cells were immediately recovered in pre-warmed medium and gently split-transferred into 24-well plates (Corning). One day after nucleofection, a medium change was performed, and further medium changes were performed every 2–3 days. To quantify knockout rates from bulk cultured cells, genomic DNA was extracted using NucleoSpin Tissue XS columns (Macherey-Nagel). Polymerase chain reactions (PCR) were performed on 1–10 ng of gDNA, formulated with 0.5 µM forward and reverse primers, 10 µl 2X buffer, and 0.5 U of Gflex Thermococcus DNA polymerase (Takara) in a 20 µl reaction. The PCR products were separated on an agarose gel via electrophoresis, and fragments corresponding to the expected amplification target were cut and gel-purified fragments were subjected to Sanger sequencing (FASMAC, Japan) using the forward primer (Table S2). The Tracking of Indels by Decomposition (TIDE) algorithm (Brinkman et al., 2014) was used to calculate indel frequency.

### Peripheral blood analysis

Peripheral blood was collected using a heparin tube and the total number of blood cells was enumerated using an automated hemocytometer MEK-6450 (Nihon Kohden). For chimerism and lineage analysis, erythrocytes were lysed in NH4Cl solution. The resulting lysed blood cells were stained with Gr1-PE, CD11b-PE, CD4-APC, CD8a-APC, CD45R[B220]-APC/eFluor 780, CD45.1-PE/Cy7 and CD45.2-BV421 for C57BL/6 mice samples, and human CD45-APC/Cy7, mouse CD45.1-e450, human CD33-PE/Cy7, and CD3/CD19-APC for human samples. The stained cells were then resuspended in 200 µL PBS/PI prior to recording events on a FACSVerse (BD) analyzer using the appropriate filters and settings.

### Akaluc vector transduction

Cultured cells underwent transduction with a VSV-G pseudotyped lentiviral vector carrying an mNeonGreen-P2A-Akaluc transgene under the regulation of the human ubiquitin C (UbC) promoter at a multiplicity of infection (MOI) of 300. A medium change was performed one day after transduction, and further medium changes were performed every 2–3 days.

### Cell counting and sample preparation for flow cytometry

Cell counting was carried out utilizing an automated cell counter (Countess II cytometer, Thermo Fisher Scientific). For hematopoietic stem and progenitor cells in the post-transplant bone marrow and spleen, cells were incubated with an anti-Lineage antibody cocktail consisting of biotinylated Gr1[LY-6G/LY-6C], CD11b, CD4, CD8a, CD45R[B220], IL7-R, and TER119. This was followed by staining with streptavidin-APC/eFluor, cKit-APC, Sca1-BV605, CD41-BV510, FcgR-PE, CD150-PE/Cy7, CD105-BV786, and CD34-PB. For analysis of mature cells, cells were stained with CD4-APC, CD8-APC, B220-APC/Cy7, CD45.1-PB, Gr1-PE, CD11b-PE, and TER119-PE/Cy7. The stained cells were then resuspended in 200 µL PBS/PI and analyzed using FACS Verse analyzer and FACS AriaIII cell sorter. For sorting of murine HSCs and exCMPs after culture, cultured bulk cells were stained with an anti-Lineage antibody

cocktail consisting of biotinylated Gr1[LY-6G/LY-6C], CD11b, CD4, CD8a, CD45R[B220], IL7-R, and TER119, followed by staining with streptavidin-BV421, cKit-APC, Sca1-APC/Cy7, CD150-PE/Cy7, and CD201-PE for cultured HSCs, and streptavidin-APC/eFlour, cKit-APC, Sca1-PE, FcgR-PE/Cy7, and CD34-PB for exCMPs. For sorting of UNexCMP, cultured bulk cells were stained with an anti-Lineage antibody cocktail consisting of biotinylated Gr1[LY-6G/LY-6C], CD11b, CD4, CD8a, CD45R[B220], IL7-R, and TER119, followed by staining with streptavidin-APC/eFlour, cKit-APC, Sca1-PE/Cy7, FcgR-FITC, and MHC ClassI-PE. For sorting of human exCMPs, cultured CD34<sup>+</sup> cells were stained with FITC anti-human Lineage Cocktail, CD34-APC, CD38-PE/Cy7, CD45RA-APC/Cy7, and CD123-PE. For sorting of human UNexCMPs, cultured CD34<sup>+</sup> cells were stained with CD34-APC, CD38-PE/Cy7, CD45RA-APC/Cy7, CD123-PE, and HLA-A,B,C-PB. To analyze mature cells post-transplantation of human exCMPs, the cells were stained with human CD45-APC/Cy7, mouse CD45.1-e450, human CD33-PE/Cy7, and CD3/CD19-APC, followed by re-suspension in 200 µL of PBS/PI before recording events on a FACSVerse (BD) analyzer using the appropriate filters and settings.

### In vivo luminescence imaging

For 3D luminescence imaging of post-transplant mice, an IVIS Spectrum CT (Caliper Life Sciences) was employed, while 2D luminescence imaging was performed using IVIS Lumina Series III and IVIS Spectrum. Mice were anesthetized with isoflurane and administered 50µL of TokeOni (15 mM, Kurogane Kasei Co., Ltd.) intraperitoneally, followed by placement in an IVIS *in vivo* imaging system (PerkinElmer). Images were captured after 5 min using appropriate binning and exposure settings. Luminescence signal intensities were analyzed using Living Image Software. To measure the luminescence signal intensity of the spleen, the ROI position for each mouse was fixed, and the temporal change of the average luminescence intensity at the same position was analyzed.

### RNAseq analysis

For RNAseq analysis, 10000 cells of exCMPs or fCMPs were sorted into 1.5 mL tubes and lysed in 600 µL Trizol LS reagent (Thermo Fisher Scientific). Subsequently, RNA purification, library preparation, and next-generation sequencing were carried out by Tsukuba i-Laboratory, LLC. Libraries were generated using the SMARTer cDNA synthesis kit (Takara) and the high-output kit v2 (Illumina), followed by sequencing on a NextSeq 500 sequencer (Illumina) at 2 × 36 paired end reads. DESeq2 package in R (Love et al., 2014) was utilized for data normalization and comparative analysis, and genes with an adjusted  $p < 0.05$  were considered differentially expressed. Enrichment analysis of differentially expressed genes was carried out using the gene set enrichment analysis (GSEA) functions in the ClusterProfiler package (Wu et al., 2021) using molecular signature database (MSigDB) gene ontology cellular component ontology, reactome pathway database, and hallmark genesets. Heatmaps were generated using the ComplexHeatmap package (Gu et al., 2016).

### Single-cell multiome analysis

Fresh CMPs, exCMPs and SPaCMPs were collected for single-cell RNA and ATAC sequencing. Fresh CMPs were directly collected from BM, exCMPs were collected from HSCs cultured for 7 days and SPaCMPs were collected from the spleen 9 days after HSC transplantation. Libraries were prepared using the Single Cell Multiome ATAC + Gene Expression Reagent Bundle (10x Genomics) and sequenced on an Illumina NovaSeq X platform. Sequencing data were mapped to the reference genome using CellRanger. Subsequent analysis was conducted using the Seurat and Signac R packages. Quality control filtering was applied to retain cells with nFeature\_RNA greater than 200 and less than 7000, a mitochondrial gene percentage less than 30%, nCount\_ATAC less than 400,000 and nCount\_ATAC greater than 1000. Data normalization and scaling were performed using the NormalizeData and ScaleData functions, respectively. For integration of sample data, the Harmony package was utilized to correct for batch effects and align the datasets. Dimensionality reduction was achieved through Principal Component Analysis (PCA) using the RunPCA function, followed by Uniform Manifold Approximation and Projection (UMAP) using the RunUMAP function. Cell clustering was conducted using the FindNeighbors, and FindClusters functions with a resolution parameter set to 0.3. Additionally, cell cycle regression was incorporated into the analysis to account for cell cycle effects.

### Transplantation assay

Cell transplantation via intravenous injection was conducted in irradiated (8.0 Gy) C57BL/6-CD45.2 recipient mice, along with  $5 \times 10^5$  C57BL/6-CD45.1/CD45.2 whole bone marrow competitor cells, using cultured cells at indicated cell doses. Secondary bone marrow transplants were performed by extracting WBM cells from the primary recipient and transplanting  $1 \times 10^6$  cells into lethally irradiated secondary recipients. For UNexCMP allo transplantation assay, BALB/c mice were treated with 10 µL anti-asialo GM1 antibody (Cedarlane Laboratories Ltd.) 2 days before transplantation. For xenotransplantation assays, human exCMPs were transplanted into sublethally irradiated (2.0 Gy) 8-10-week-old immunodeficient NOG mice.

### DPP4 activity assay

50000 cells of exCMPs or fCMPs were lysed in Glo Lysis Buffer (Promega), and DPP4 enzyme activity was then determined by means of the DPPIV-Glo Protease Assay (Promega). In order to execute the DPP4 inhibition assay, Diprotin A TFA (50 µM, MedChemExpress) was added to the lysate. The resulting luminescence signal was then recorded using a microplate reader (Varioskan LUX, Thermo Fisher Scientific).

***In vivo G-CSF reactivity assay***

Ten thousand cells each of C57BL/6-CD45.1 exCMP and C57BL/6-CD45.1/CD45.2 fCMP were co-transplanted into irradiated (8.0 Gy) C57BL/6-CD45.2 recipient mice. Subsequently, 5 µg of G-CSF (Kyowa Kirin Co., Ltd.) was intraperitoneally administered on days 1, 3, and 5 post-transplantation. On day 7, the mice were sacrificed, and the spleen cells were analyzed.

**QUANTIFICATION AND STATISTICAL ANALYSIS**

Information concerning the statistical tests applied, the number of subjects and groups are mentioned in the figure legends. The asterisks in the figures represent statistical significance levels, defined as follows: \* $p < 0.05$ , \*\* $p < 0.01$ , \*\*\* $p < 0.001$ , and \*\*\*\* $p < 0.0001$ . Student's t-tests, one- and two-way analysis of variance (ANOVA) were executed using Prism (version 9.5, Graphpad). Standard deviations are represented by error bars. For statistical analysis related to RNAseq, R version 4 (R Core Team, 2020) along with the fitting package were utilized. Illustrations and diagrams were produced utilizing BioRender (<https://www.biorender.com/>).